Check for updates

JGR Oceans

RESEARCH ARTICLE
10.1029/2021JC018374

Increasing Wave Energy Moves Arctic Continental Shelves Toward a New Future

John Malito[1], Emily Eidam[1], and Jaap Nienhuis[2]

[1]Department of Earth, Marine, and Environmental Sciences, University of North Carolina, Chapel Hill, NC, USA, [2]Department of Physical Geography, Utrecht University, Utrecht, The Netherlands

Key Points:

- A morphodynamic model was developed to explore feedbacks between Arctic continental shelves and growing sea states related to sea-ice losses
- On a higher-relief shelf section, stronger waves drove offshore sediment transport and mid-shelf deposition which regulated wave energy
- A lower-relief shelf section was relatively insensitive to morphologic adjustment under larger waves due to effective wave attenuation

Supporting Information:

Supporting Information may be found in the online version of this article.

Correspondence to:

E. Eidam,
emily.eidam@oregonstate.edu

Citation:

Malito, J., Eidam, E., & Nienhuis, J. (2022). Increasing wave energy moves Arctic continental shelves toward a new future. *Journal of Geophysical Research: Oceans*, *127*, e2021JC018374. https://doi.org/10.1029/2021JC018374

Received 23 JAN 2022
Accepted 27 JUL 2022

Author Contributions:

Conceptualization: John Malito, Emily Eidam, Jaap Nienhuis
Data curation: John Malito, Emily Eidam
Formal analysis: John Malito, Emily Eidam, Jaap Nienhuis
Investigation: John Malito, Emily Eidam, Jaap Nienhuis
Methodology: John Malito, Emily Eidam, Jaap Nienhuis
Project Administration: Emily Eidam, Jaap Nienhuis
Supervision: Emily Eidam, Jaap Nienhuis
Validation: John Malito, Jaap Nienhuis
Visualization: John Malito
Writing – original draft: John Malito
Writing – review & editing: John Malito, Emily Eidam, Jaap Nienhuis

© 2022. American Geophysical Union. All Rights Reserved.

Abstract Arctic continental shelves, including the Alaskan Beaufort Shelf (ABS), are experiencing declines in sea ice coverage leading to increasingly energetic sea states and coastal erosion. In this study we investigated the morphologic response of the ABS to increasing wave energy, and how shelf profile adjustments modify wave energy propagating toward the coast. We developed a 2D cross-shelf morphodynamic model using Delft3D and tested shelf response to a present-day wave climate and a future Arctic wave climate projected under the RCP8.5 climate-change scenario. Simulations lasting 1000 years were conducted for relatively steep (Flaxman Island, AK, slope 0.0008) and flat (Harrison Bay, AK, slope 0.0003) cross-shelf profiles. We found that morphologic evolution and regulation of future waves depends primarily on existing shelf morphology. On the steeper profile, RCP 8.5 waves drove sediment erosion at 0–15 m water depth and redeposition at 15–30 m water depth. Over 1000 years, this redistribution of sediment from the inner to middle shelf resulted in a 7.6% reduction in wave heights at the 2 m isobath. This morphologic adjustment represented a regulatory feedback in which shallowing of the middle shelf led to attenuation of waves reaching the inner shelf. In contrast, effective wave attenuation across the flatter and wider Harrison Bay section limited cross-shelf transport and morphologic change under both wave climates. Together our results suggest that coastal changes in response to the growing Arctic wave climate may be dependent on shelf morphology, and even mitigated in some regions by morphologic adjustment.

Plain Language Summary In recent decades, declining Arctic sea ice has led to increasingly energetic waves that persist for longer periods throughout the year, thereby accelerating coastal erosion and posing a threat to coastal communities and ecosystems. However, waves are modified as they travel across the continental shelf, making the shelf a key factor in how shorelines are impacted by wave energy. A sediment transport model was developed to test how present-day and projected future waves can impact shelf evolution, and how shelf geometry can influence the character of waves reaching the coast. Our results showed that a relatively steep Arctic shelf section was more sensitive to the growing wave climate. Enhanced waves drove greater erosion on the inner shelf and deposition of these sediments on middle shelf. The redistribution of sediments from the inner shelf to the middle shelf led to attenuation of projected waves as the shelf evolved over time, reducing the relative impact of greater future waves. In contrast, a relatively flat shelf section damped wave energy, and reduced the potential for changes in the continent shelf shape. These results suggest that the shape of a continental shelf can impact how increasingly large waves are felt at the coastline.

1. Introduction

Arctic air temperatures are increasing at rates over twice that of the Northern Hemisphere average (Box et al., 2019). Because of climate-driven environmental changes, the Arctic is experiencing rapid declines in sea ice extent (Barnhart et al., 2016), widespread permafrost melt (Obu et al., 2017), accelerated coastal erosion (Gibbs & Richmond, 2017), and coastal flooding (Arp et al., 2010). Furthermore, sea states in the Arctic have been increasing as a function of sea ice decline (Casas-Prat & Wang, 2020; Thomson et al., 2016; Wang et al., 2015). Though it is somewhat unclear whether Arctic storms have been increasing in duration and intensity (Day et al., 2018; Kistler et al., 2001; Sepp & Jaagus, 2011), delayed freeze-up has caused the open-water season to coincide more with the already stormy months of October and November (Thomson et al., 2016). As a result, Arctic coastal communities, infrastructure, and ecosystems are increasingly vulnerable to environmental hazards (Manrique et al., 2018). Effects of climate change on Arctic coastal dynamics remain poorly understood, particularly the feedbacks between continental shelf sediment dynamics and sea states that impact Arctic coastal systems on centennial to millennial time scales.

21699291, 2022, 9, Downloaded from https://agupubs.onlinelibrary.wiley.com/doi/10.1029/2021JC018374 by Utrecht University Library, Wiley Online Library on [21/10/2022]. See the Terms and Conditions (https://onlinelibrary.wiley.com/terms-and-conditions) on Wiley Online Library for rules of use; OA articles are governed by the applicable Creative Commons License

21699291, 2022, 9, Downloaded from https://agupubs.onlinelibrary.wiley.com/doi/10.1029/2021JC018374 by Utrecht University Library, Wiley Online Library on [21/10/2022]. See the Terms and Conditions (https://onlinelibrary.wiley.com/terms-and-conditions) on Wiley Online Library for rules of use; OA articles are governed by the applicable Creative Commons License

The impact of storm events on Arctic coastal erosion has been well documented (Arp et al., 2010; Barnhart et al., 2014; Sturtevant et al., 2004), but the coupling between long-term Arctic shelf evolution and storm transformation beyond the shoreline is seldom addressed. Waves are transformed as they propagate across a shelf, undergoing refraction, shoaling, diffraction, and dissipation before reaching the coast (Ardhuin et al., 2003; Blanco-Chao et al., 2019; Lacy & MacVean, 2016). Wave energy is presently a key erosive mechanism during the open-water season along Arctic coastlines. Similarly, storm surge at the coast can lead to thermal erosion of ice-rich coastal bluffs (Héquette & Hill, 1993; Hill et al., 1991). The geometry of the cross-shelf profile exerts a strong control on both wave transformation and storm surge through bottom friction (Dean & Dalrymple, 2004). In turn, shelf morphology is dictated largely by cross-shelf gradients in wave-induced bed stresses leading to sediment transport and adjustment of the shelf profile shape (C. K. Harris & Wiberg, 2002). Morphologic change on wave-dominated shelves is determined by the cumulative sum of sediment transport by storm waves balanced by partial recovery during fair-weather periods (Anderson et al., 2010; Ogston & Sternberg, 1999), and wave events are important drivers of sediment transport (Hill et al., 1991; Sturtevant et al., 2004). The result is a feedback between hydrodynamic forcings and sediment transport that determines the shape and stability of the shelf profile over long timescales (Fagherazzi & Overeem, 2007; Friedrichs & Wright, 2004).

In this study, we evaluated the potential morphologic response of two sections of the Alaskan Beaufort Shelf (ABS) to an increased wave climate, and how wave attenuation impacts sediment transport across shelf profiles of different geometries. Because waves impact the potential for coastal erosion, we also explored the character of waves delivered to the inner shelf after transformation across the middle and outer shelf. We chose to study two sections of the Alaskan Beaufort Shelf, which can serve as an analog for numerous Arctic marine environments undergoing these climate-driven changes.

We developed a cross-shelf morphologic model using Delft3D-FLOW to explore the long-term evolution of the ABS under present and project wave climates, with emphasis on the coupling between hydrodynamic forcings, cross-shelf sediment transport, and morphologic adjustment of the shelf profile. We analyzed two cross-shelf transacts of the ABS, one presently steep shelf ("Flaxman Island" transect) and one that is relatively shallow ("Harrison Bay" transect). For these two transects, we compared 1000-year cross-shelf evolution under present-day wave climate versus a projected wave climate modeled under the Representative Concentration Pathway 8.5 forcing scenario for climate change in 2100 (hereafter referred to as RCP8.5 waves). The millennial time-scale simulations allowed for morphodynamic processes to stabilize after the application of waves and led to the time-steady changes. Given the importance of storm waves on the evolution of Arctic shelves, a representative storm was also applied to the modeled shelf profiles to investigate the coupling between shelf geometry and the potential for storm-driven sediment transport.

2. Background

2.1. Alaskan Beaufort Shelf

The Alaskan Beaufort Shelf (ABS) spans 600 km of the northern Alaskan coast, between Point Barrow and the Canadian border (Figure 1). With shelf widths ranging from 50 to 100 km, the ABS is narrow relative to the average Arctic shelf width of 104 km (P. T. Harris & Macmillan-Lawler, 2016; Norton & Weller, 1984). Typical slopes of the ABS fall at or below the global average of 1.8×10^{-3}. Therefore, the ABS can be considered an "intermediate shelf" based on global average slopes and widths (P. T. Harris et al., 2014). Breaks in shelf slope can occur at various isobaths as a function of sea ice zonation (Reimnitz et al., 1978). A shallow bathymetric platform, or "bench," is common inshore of the 2 m isobath and is likely related to deposition promoted by shorefast ice (Reimnitz et al., 1985) or submerged coastal lagoons (Gibbs & Richmond, 2017). The present shoreline position and shelf morphology are the products of 140 m of sea level rise during the Holocene (Héquette, Ruz, & Hill, 1995; Hill et al., 1985). The rate of relative sea level rise at Prudhoe Bay, AK between 1988 and 2020 was 3.23 ± 1.51 mm/yr (NOAA, 2022).

The ABS is sheltered by sea ice between October and June, leaving a brief window of time in which open-water sediment-transport processes can occur. Increasing wave energy throughout the summer and storm waves in the fall can generate high bed stresses, storm surge, and changes in near-bed currents (Barnhart et al., 2014; Pickart et al., 2013). Arctic-born storms approaching the ABS from the northwest are the principal drivers of sediment transport during open-water season, generating coastal setup and exposing the coastline to intense wave action

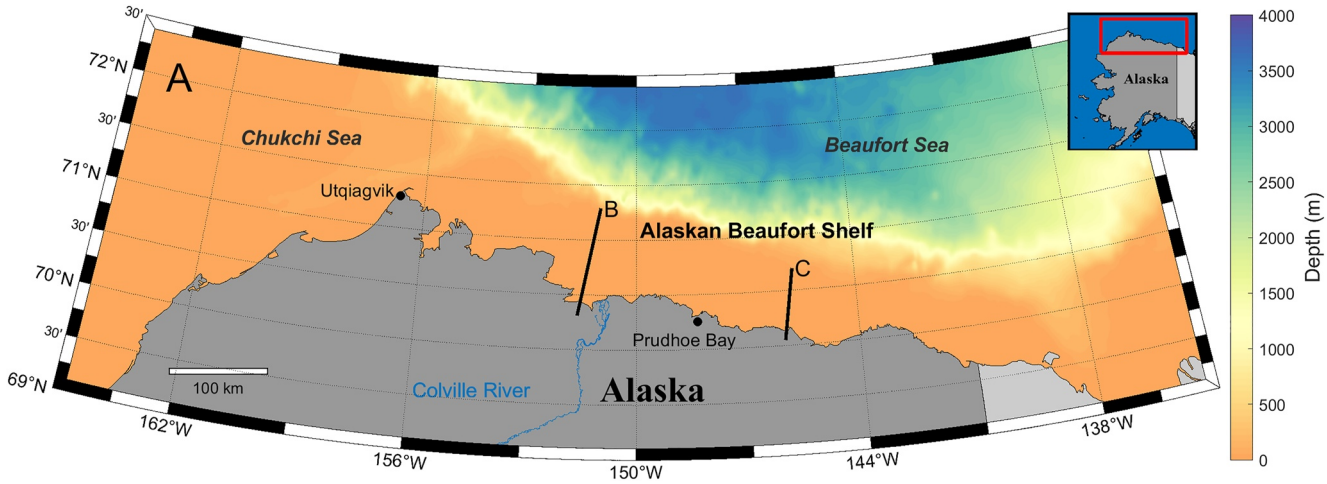

Figure 1. (a) An overview of the focus area of this study, the Alaskan Beaufort Shelf, featuring the two cross-shelf transects with contrasting profile slopes, near (b) Harrison Bay and (c) the Flaxman Islands. Average transect slope is calculated between the two white circles. Bathymetric data were gathered from the publicly available International Bathymetric Chart of the Arctic Ocean repository (Jakobsson et al., 2020), and vessel-based surveys (see Data Accessibility note).

(Héquette & Hill., 1993; Manson & Solomon, 2007). In fair weather conditions, winds blow predominantly from the east with speeds <6 m/s and do not develop significant coastal setdown or wave action (Héquette & Hill, 1993). Though climate-driven changes to storm dynamics remain uncertain (Day et al., 2018), the expanding duration of the open-water season can expose the shoreline to more storms per year. Since storms play a large role in coastal erosion, increased exposure to storm energy could lead to greater retreat rates (Barnhart et al., 2014; Gibbs et al., 2015; Lynch et al., 2004; Obu et al., 2017).

Much of the ABS coastline consists of ice-rich bluffs or barrier island systems characterized by loose, unconsolidated, and easily erodible sediments (Gibbs & Richmond, 2017; Hequette & Barnes, 1990). Approximately 80% of the coastline is thought to be erosional (Harper, 1990). Erosion rates on the ABS average between 1 and 2 m/yr (Gibbs et al., 2011; Harper, 1990; Reimnitz et al., 1985) but are locally variable, with maxima of >20 m/yr (Obu et al., 2017). During the open-water season, permafrost-rich coastlines are exposed to both mechanical and thermal erosive energy by means of wave action and direct exposure to warm seawater, respectively (Barnhart et al., 2014). Coastal erosion is thought to contribute 7 to 10 times more sediment than the Colville River, the other principal source of sediment to the ABS (Rachold et al., 2000; Reimnitz et al., 1988). Observed accelerations to Arctic coastal retreat have implications for both sediment supply to the shelf and the adjustment of the nearshore profile, especially given that coastal erosion can occur in the absence of wave erosion (i.e., by thermal processes).

Currents on the shelf are principally shore-parallel and closely coupled to an evenly distributed bimodal wind climate during the open-water season (Barnes & Reimnitz, 1982; Forest et al., 2016; Weingartner et al., 2009). Along-shelf currents on the ABS can exceed 20 cm/s during the open-water season and 10 cm/s during periods of ice cover, but long-term averages are typically near zero due to the bimodal wind climate (Weingartner et al., 2009). Cross-shelf currents are typically <3 cm/s (Weingartner et al., 2017), but are capable of exporting sediments suspended by wave action from the coast via advection during storm events (Héquette et al., 2001; Héquette & Hill, 1993). Furthermore, downslope diffusion of sediments transported by shore-parallel currents may contribute to cross-shelf sediment transport (Hill et al., 1991). The coastal ocean is microtidal (Okkonen, 2016), and tides do not play a significant role in sediment transport on the shelf (Weingartner et al., 2009).

Ice processes are an additional mechanism of sediment transport, especially inshore of the 45 m isobath where ice keels can scour and rework seabed sediments (Barnes et al., 1987; Harper, 1990). Keel scour occurs within the "Stamukhi zone," where landfast ice and pack ice collide and the resulting ice ridges scour the seabed (Héquette, Desrosiers, & Barnes, 1995; Reimnitz & Maurer, 1978). Bulldozing and scouring of sediments can also occur in the nearshore zone and beach (Barnes & Reimnitz, 1982). However, the majority of keel-driven sediment transport occurs over short distances, and in the along-shore direction, acting more as an agent of seabed mixing than significant transport (Héquette, Desrosiers, & Barnes, 1995; Hill et al., 1991). In winter months, wave

21699291, 2022, 9, Downloaded from https://agupubs.onlinelibrary.wiley.com/doi/10.1029/2021JC018374 by Utrecht University Library, Wiley Online Library on [21/10/2022]. See the Terms and Conditions (https://onlinelibrary.wiley.com/terms-and-conditions) on Wiley Online Library for rules of use; OA articles are governed by the applicable Creative Commons License

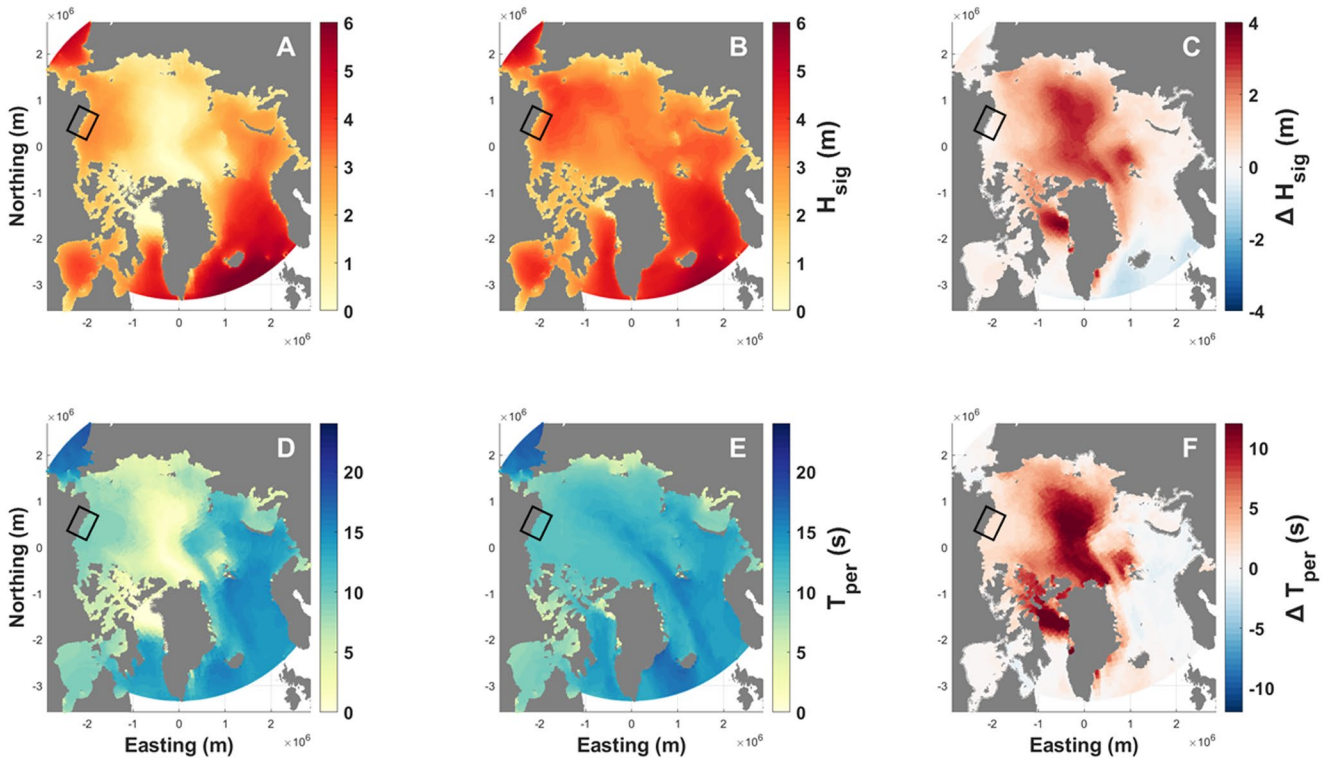

Figure 2. Pan-Arctic maps displaying hindcasted present-day (1979–2005) and projected future (2080–2100 under RCP8.5 forcing scenario) wave parameters. (a and b) Significant wave height (m) for present and future wave climates, respectively. (c) Difference in wave heights between (a and b). (d and e) Peak wave period (s). (f) Difference in peak wave period. These values are averaged over the month of September of each year, the month with the lowest sea ice cover. The Alaskan Beaufort Shelf is denoted by the black rectangle. Data from Casas-Prat et al. (2018).

and surge development are suppressed, and shorefast and ground ice limit movement of sediments (Manson & Solomon, 2007). Extended periods of stability are sometimes interrupted by events where ice coverage shifts and reworks seabed sediments (Reimnitz et al., 1985). Sediments on the ABS are dominated by fine-grained sand and mud, but size distributions are highly variable (Fischbein, 1987; Harper, 1990). Distributions of gravels, sands, silts, and clays are patchy (Barnes et al., 1980) due to ice processes which stir and expose sediments that were deposited under a different hydrodynamic regime (Barnes & Rearic, 1985; Barnes et al., 1980).

2.2. Arctic Wave Climate

The primary control on Arctic sea states is the presence of sea ice (Casas-Prat & Wang, 2020; Hill et al., 1991; Thomson et al., 2016; Wang et al., 2015). Sea ice impacts the sea state through three linked variables: (a) fetch over which waves can develop (e.g., Smith & Thomson, 2016); (b) duration of open-water throughout the year (e.g., Barnhart et al., 2014; Overeem et al., 2011); and (c) attenuation of waves in the presence of sea ice (e.g., Hošeková et al., 2020; Thomson & Rogers, 2014). The net effect observed over the last several decades has been an increase in wave height, period, and duration of wave exposure due to climate-driven reductions to sea ice (Thomson et al., 2016).

Between 1970 and 1999, Arctic Ocean wave periods have increase at a rate of 3%–4% per year, and significant wave heights have increased at a rate of 0.3%–0.8% per year (Wang et al., 2015). These trends are expected to continue into the future (Figure 2; Casas-Prat & Wang, 2020). The annual duration of open-water season is presently expanding at a rate of ± 0.5 days per year (Thomson et al., 2016), and by 2050, the entire Arctic coastline is expected to experience between 60 and 100 additional days of open-water per year as compared to 2016 (Barnhart et al., 2016). Increases in wave energy and a longer open-water season are expected to impact coastal erosion (Barnhart et al., 2014; Stroeve et al., 2007), and also allow for greater sediment-transport capacity on the continental shelf.

21699291, 2022, 9, Downloaded from https://agupubs.onlinelibrary.wiley.com/doi/10.1029/2021JC018374 by Utrecht University Library, Wiley Online Library on [21/10/2022]. See the Terms and Conditions (https://onlinelibrary.wiley.com/terms-and-conditions) on Wiley Online Library for rules of use; OA articles are governed by the applicable Creative Commons License

21699291, 2022, 9, Downloaded from https://agupubs.onlinelibrary.wiley.com/doi/10.1029/2021JC018374 by Utrecht University Library, Wiley Online Library on [21/10/2022]. See the Terms and Conditions (https://onlinelibrary.wiley.com/terms-and-conditions) on Wiley Online Library for rules of use; OA articles are governed by the applicable Creative Commons License

2.3. Shelf Morphodynamics

Continental shelves are a zone of transition between the deep ocean and the shoreline where wave height attenuation occurs as waves propagate toward the coast.

The principal mechanism for sediment transport and morphologic change on a wave-dominated shelf such as the ABS is wave-induced sediment resuspension and subsequent advection by currents. Although currents flow predominantly in the along-shelf direction (Dufois et al., 2008; Hill et al., 1991; Wright, 2012), cross-shelf sediment fluxes typically have higher gradients and thus exert a stronger control on the geometry of the shelf profile (C. K. Harris & Wiberg, 2002). A source of cross-shelf gradients in sediment fluxes is from the depth-dependence of wave-induced bed shear stresses, because wave orbital velocities increase with decreasing water depth.

The resulting morphologic evolution of the shelf can vary from the shortest timescale, the wave orbital motion, to the most extreme and infrequent storms (Nittrouer & Wright, 1994). The long-term evolution of a shelf profile is determined by the sum of short-term adjustment to storm events balanced by recovery during calmer weather (Anderson et al., 2010; Héquette & Hill, 1993; Ogston et al., 2000).

On long timescales, the wave-induced cross-shelf bedload transport is directed onshore and can be balanced by offshore-directed downslope transport (Ortiz & Ashton, 2016). This balance leads to a concave-up shelf profile.

Alternatively, regions dominated by the supply of fine-grained sediments can develop a convex-up shelf profile (C. K. Harris & Wiberg, 2002; Friedrichs & Wright, 2004). Fine-grained sediment mobilized by waves in shallow water can be advected to greater depths (sometimes by wave-supported gravity flows) where shear stresses are relaxed. The resultant profile can be maintained in equilibrium at long-timescales by a balance between wave energy dissipation in shallow water and gravity-driven transport to deeper water (Friedrichs & Wright, 2004).

Natural shelf systems experience a mixture of processes that form concave-upward profiles (in regions where wave energy is high and sediments are coarse enough for bedload transport to be important) and convex-upward profiles (in regions where sediment supply is high and sediments are fine grained). In addition, there exist multiple factors that might cause continental shelves to be out of equilibrium, especially in northern Alaska. The ongoing adjustments to sea-level rise following the Last Glacial Maximum have been more rapid compared to many temperate coastlines (Overeem et al., 2022). There have also been variations in wave climate and sediment supply. In addition, the present-day morphology varies along the ABS, despite broadly similar wave forcing and sea level history, which can also influence future change.

The growing Arctic wave climate can be expected to create a state of further disequilibrium in which enhanced wave energy alters the shelf morphodynamics. The ABS presently has a concave-upward profile with relatively steep inner shelf slopes (1×10^{-3}) transitioning to gentler slopes on the middle shelf (1×10^{-4}). This profile shape is typical of shelves where wave energy is the principal driver of sediment transport supply is limited (Friedrichs & Wright, 2004; Ortiz & Ashton, 2016).

An increase in wave height and deepening of the wave base can mobilize sediments at greater depths across the shelf. As a result of an increased wave climate, the profile may be adjusted by sediment diffusion from areas of higher wave energy dissipation to those with lower wave energy dissipation (Friedrichs & Wright, 2004), a process which will steepen the shelf profile (Ortiz & Ashton, 2016).

Although we have a good understanding of the principal processes behind shelf morphodynamics, the potential impacts of an enhanced wave climate on the Arctic shelf, with its complex present-day morphology and large anticipated changes, remain poorly known.

3. Methods

3.1. Model Setup

A 2D cross-shelf morphodynamic model was developed using Delft3D (Lesser et al., 2004; Roelvink & Walstra, 2004) to evaluate the morphological response of the ABS to a representative present-day and RCP8.5 wave climate. Delft3D is a commonly used hydro + morphodynamic model for a wide range of coastal engineering and science applications, computing hydrodynamic and sediment transport processes simultaneously as described by Lesser et al. (2004). Sediment transport formulations outlined by van Rijn (2007) were used

21699291, 2022, 9, Downloaded from https://agupubs.onlinelibrary.wiley.com/doi/10.1029/2021JC018374 by Utrecht University Library, Wiley Online Library on [21/10/2022]. See the Terms and Conditions (https://onlinelibrary.wiley.com/terms-and-conditions) on Wiley Online Library for rules of use; OA articles are governed by the applicable Creative Commons License

Table 1
Initial Delft3D Model Parameters

	Model parameters	
Location	Harrison Bay, AK	Flaxman Island, AK
Morphology		
Average slope (m/m)	3.0×10^{-4}	8.0×10^{-4}
Non-cohesive d_{50} (μm)	110	81
Cohesive settling velocity (mm/s)	1.0	1.0
Volumetric sand fraction	29	12
Volumetric mud fraction	71	88
Sand porosity	0.40	0.40
Mud porosity	0.60	0.60
Sand critical shear stress τ_c (N/m^2)	0.23	0.23
Mud critical shear stress τ_c (N/m^2)	0.50	0.50
Representative Tides		
Diurnal amplitude (cm)	3.7	6.5
Semidiurnal amplitude (cm)	1.7	2.1

Note. Tidal components do not represent total observed tidal amplitudes on the ABS, but instead are isolated diurnal and semidiurnal components used to stabilize the flow field.

to calculate bedload and suspended load transport influenced by waves and currents. Phase-averaged wave propagation from offshore toward the coast are computed within Delft3D-FLOW using its roller model (Deltares, 2014).

3.2. Model Domain

Interactions between shelf geometry and wave propagation were analyzed by using two separate bathymetric cross-shore transects from the ABS. The ABS at Harrison Bay (Figure 1b) represents a broad and flat shelf section with a slope of 3.0×10^{-4} m/m. In contrast, the shelf section at Flaxman Island (Figure 1c) represents a relatively steep section of the ABS, with a slope of 8.0×10^{-4} m/m. A single regional high-resolution bathymetric product is not presently available. Therefore, bathymetric transects from multiple sources were merged and smoothed from 0 to 80 m depth to create a single representative transect for each profile location. High resolution (25 m) bathymetric data (see Data Availability) were used for the inner shelf, ship-based 5-cm resolution bathymetric data were used for the middle shelf (see Data Availability), and International Bathymetric Chart of the Arctic Ocean (IBCAO) (Jakobsson et al., 2020) 200 m resolution bathymetric data were used for the outer shelf. Landward of the shoreline, a 2-m high bluff/coastal plain was extended 8 km inland to allow for coastal erosion and shelf profile translation. This bluff comprised the same sediment as the seabed (see below), and eroded or prograded based on whether offshore or onshore fluxes (respectively) dominated in the nearshore. Ice content was deemed to be beyond the scope of this study and was not modeled.

A sigma (σ) coordinate system was implemented in the Delft3D-FLOW domain. For the σ grid, 12 layers of a fixed percentage of the water column are used to represent the vertical dimension. Layer thicknesses were set to be smaller adjacent to the surface and the seabed boundary to improve model stability (Lesser et al., 2004). The cross-shelf horizontal grid resolution increased progressively with depth to adhere to the recommended Courant-Friedrichs-Lewey number for model stability (*CFL*) limit for waves of less than 10 (Deltares, 2014; Lesser et al., 2004)

$$CFL = \frac{\Delta t \sqrt{gd}}{\Delta x} \quad (1)$$

where Δt is the timestep duration (s), g is the gravitational constant, d is water depth, and Δx is the grid cell spacing in the cross-shelf dimension. Thus, cross-shelf grid cell lengths were set to 90 m at the coastline, increasing sequentially to 1,000 m at the seaward boundary (80 m depth). Thin dams with free-slip walls were added to the sides of the model domain to isolate the cross-shelf components of flow and sediment transport. The offshore boundary condition was an open astronomic boundary and the side boundaries were Neumann time-series boundaries.

Representative seabed textures were implemented for each transect using average fractions and diameters of surficial seabed samples collected in situ from cross-shelf transects near Harrison Bay, AK and Flaxman Island, AK. Sediment samples were collected aboard the R/V *Sikuliaq* in fall 2019 and fall 2020 and analyzed for grain-size distributions using a Bettersizer S3Plus laser diffraction sensor. Seabed textures on the ABS are typically patchy and spatially diverse (Barnes et al., 1980). Samples collected in this present study followed this trend, where bimodal matrices of fine sands and fine silts were present with no clear dependence on depth or location.

To construct initial bed compositions in Delft3D-FLOW, sediment populations for both transects were split into their sand (≥63) and mud (<63) populations and the overall transect-averaged grain d_{50} values and fractions were computed for each. Seabed textures implemented in the model are presented in Table 1. At Harrison Bay, the representative non-cohesive sand had a d_{50} of 109.7, with a volumetric fraction of 29%, accompanied by 71% mud. Flaxman Island was principally composed of a sandy-mud matrix, with an average d_{50} of 80.7 and volumetric sand and mud percentages of 12% and 88%, respectively. For cohesive sediments, Delft3D does not require grain

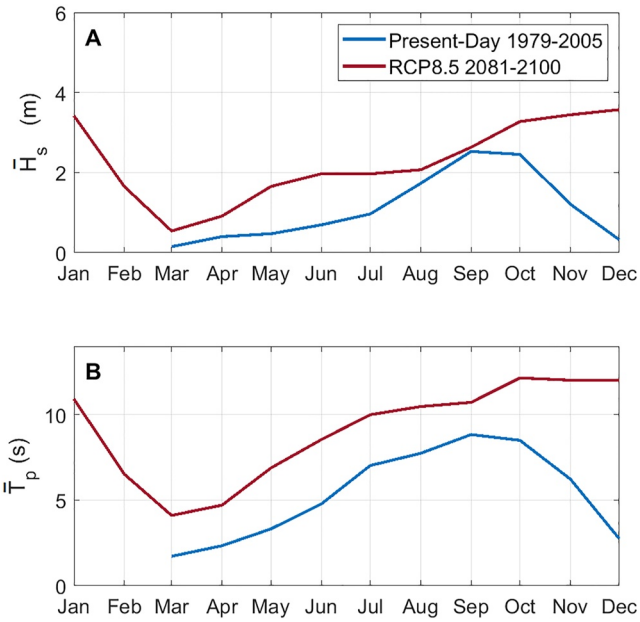

Figure 3. Time series of monthly wave parameters (a) H_s and (b) T_p scaled using Equation 2 implemented in the model. Hindcast shown in blue and projected RCP8.5 waves under climate forcing scenario RCP8.5 shown in red.

diameter in the sediment transport formulations but rather requires settling velocity (Deltares, 2014). Thus, settling velocity for the cohesive mud was set to 1 mm/s to represent flocculation of muds in saline environment (C. K. Harris & Wiberg, 2002; Sternberg et al., 1999). Additional model parameters can be found in Appendix A3.

3.3. Hydrodynamics

Two simplified wave climates were applied to the model to evaluate the influence of an increased wave climate on the ABS. The publicly available wave data set Coupled Model Intercomparison Project Phase 5 (CMIP5) included monthly averaged wave parameters for the entire Arctic over a hindcast period from 1979 to 2005 and RCP8.5 projected period between 2081 and 2100 (Casas-Prat et al., 2018). The 1979–2005 wave hindcast is hereafter referred to as present-day waves, and the projected 2081–2100 data set is referred to as RCP8.5 waves. Annual time series for both wave climates were constructed using a weighted monthly averaged wave height and wave period (Figure 3) for the ABS, and repeated at the seaward boundary of the model for the 1000-year duration of the simulations. The weighted monthly average was calculated using a scaling term, q_s, to more adequately capture the enhanced influence of larger waves in determining the equilibrium shelf profile (Ortiz & Ashton, 2016):

$$q_s \propto H_s^5 T_p^{-5} \sinh^{-5}(kz) \tag{2}$$

where H_s is significant wave height, T_p is peak wave period, k is wave number, and z is a representative shelf depth at which waves are analyzed. After computing the scaling factor, q_s, the monthly weighted average $\bar{H}_s$ and $\bar{T}_p$ can be calculated as

$$\left(\bar{H}_s, \bar{T}_p\right) = \frac{\sum (H_s, T_p)\, q_s}{\sum q_s} \tag{3}$$

where $\bar{H}_s$ and $\bar{T}_p$ are the scaled monthly wave parameters implemented in the model (Figure 3). Furthermore, though ice cover was not included explicitly in the Delft3D-FLOW model, the impacts of reduced ice in the future were represented by stronger waves and a longer open-water season in the RCP8.5 wave climate (Casas-Prat et al., 2018).

Tidal ranges on the ABS are typically less than 20 cm in amplitude and generally produce weak currents less than 3 cm/s near the seabed (Okkonen, 2016; Weingartner et al., 2017). Therefore, simple tides were implemented in the model to stabilize the flow field by extracting the principal diurnal component (M2) amplitude and semidiurnal component (O1) amplitudes and implementing them at the seaward boundary of the model domain (Table 1).

3.4. Long-Term Simulations

Model experiments were conducted to investigate the long-term effects of the present-day versus RCP8.5 wave climate on the Harrison Bay and Flaxman Island bathymetric transects. First, a bed-composition generation (BCG) trial was implemented for 2 months to allow for sediment fractionation without vertical bed-level change (van der Wegen et al., 2011). Then, the BCG output seabed textures were used as the initial conditions of a 500-year morphodynamic trial under the present-day wave condition. The outputs of this 500 year trial were used as initial conditions for subsequent analyses in order to reduce bias introduced by morphodynamic spin-up and smoothing of bathymetry. Next, sediment transport and shelf morphology were evaluated under two wave climates by conducting 1000-year trials with present-day and RCP8.5 wave conditions on both the Harrison Bay and Flaxman Island shelf transects (Figure 1).

21699291, 2022, 9, Downloaded from https://agupubs.onlinelibrary.wiley.com/doi/10.1029/2021JC018374 by Utrecht University Library, Wiley Online Library on [21/10/2022]. See the Terms and Conditions (https://onlinelibrary.wiley.com/terms-and-conditions) on Wiley Online Library for rules of use; OA articles are governed by the applicable Creative Commons License

Figure 4. ERA5 wave hindcast wave parameters (Hersbach et al., 2018), significant wave height (H_s) and peak wave period (T_p), for a storm occurring near the Flaxman Island, AK shelf section between 23 and 31 August 2020. This represents a typical ABS storm and was implemented on modeled output shelf profiles.

A morphological scaling factor (MF) was tested and implemented to reduce computational expense for these long-term simulations. Based on the assumption that hydrodynamic and morphodynamic processes are linearly related, bed erosion and deposition are multiplied by MF (Lesser et al., 2004; Roelvink & Walstra, 2004). For example, if MF = 24, 1 hr of flow computation yields one day of morphologic change (Lesser et al., 2004). After conducting a Brier Skill Score (BSS) sensitivity test using the methods outlined by Ranasinghe et al. (2011), it was determined that an MF of 100 could be used to reliably evaluate morphologic change (Appendix A1).

3.5. Storm Timescale Simulations

To investigate the influence of shelf profile geometry on the delivery of waves to the inner shelf (and resultant potential for sediment transport), a representative 7-day Arctic storm was applied to the 1000-year modeled shelf sections generated by present-day and RCP8.5 wave climates (Figure 4). Significant wave height and peak wave period time series were implemented at the seaward boundary for each model trial. The storm event lasted approximately 7 days between 24 and 31 August 2020. Significant wave heights reached a maximum of 2.5 m with heights above 2 m sustained over 2 days. Wave parameters H_{sig} and T_p from the ERA5 wave hindcast model (Hersbach et al., 2018) were retrieved for the duration of the storm on the ABS near the Flaxman Island shelf section.

4. Results

Results are presented following the sequence of morphodynamic evolution in the Arctic: (a) a climate-driven growth in wave climate, (b) resultant changes to sediment transport dynamics, (c) morphologic adjustment of the cross-shelf profile, (d) and the feedback between the evolving shelf profile and wave propagation toward the coast. Videos of shelf evolution modeled in this study can be found in Supporting Information S1.

4.1. Long-Term Evolution of Arctic Shelves

4.1.1. Waves and Wave-Induced Bed Stresses

A climate-driven growth in wave heights was simulated by imposing representative present-day and RCP8.5 wave climates at the seaward boundary of the model in two separate trials (Table 2). A change in the duration of the open-water season was also represented by imposing present-day waves for 6 months and RCP8.5 waves for 12 months (Figure 3).

Wave attenuation was calculated as the percent decrease in wave heights between the offshore boundary and the 10 m isobath. At Flaxman Island, wave heights attenuated 15% and 23% for present-day and RCP8.5 wave climates, respectively. On the shallower, lower-gradient Harrison Bay shelf, wave heights attenuated 38% and 55% for present-day and RCP8.5 wave climates, respectively (Table 2).

The increase in significant wave heights across the shelf (as a consequence of imposing RCP8.5 waves) was also different for each shelf. For Flaxman Island, average cross-shelf wave heights increased 136% between present-day and RCP8.5 scenarios, versus only 115% on the gently sloping Harrison Bay transect (Table 2). In other words, the same climate-driven increase in wave heights led to a larger increase in wave heights across Flaxman Island than Harrison Bay, due to differences in wave attenuation.

On both transects, wave-induced shear stresses were greater in the RCP8.5 scenario (Figures 5e and 5f) because wave orbital velocities scale with the different wave heights imposed. Between 25 and 5 m depth, average bed shear stresses were greater in the RCP8.5 scenario than in the present-day scenario: 0.56 ± 0.15 N/m^2 (present-day) versus 1.66 ± 0.07 N/m^2 (RCP8.5) at Harrison Bay and 0.97 ± 0.42 N/m^2 (present-day) versus 2.90 ± 0.66 N/m^2 (RCP8.5) at Flaxman Island (Table 2). Wave-induced bed shear stresses tripled between present-day and RCP8.5 wave climates across both shelves. Bed stresses at Flaxman Island were typically double that of Harrison Bay because less wave attenuation occurred across the steeper transect.

21699291, 2022, 9, Downloaded from https://agupubs.onlinelibrary.wiley.com/doi/10.1029/2021JC018374 by Utrecht University Library, Wiley Online Library on [21/10/2022]. See the Terms and Conditions (https://onlinelibrary.wiley.com/terms-and-conditions) on Wiley Online Library for rules of use; OA articles are governed by the applicable Creative Commons License

21699291, 2022, 9, Downloaded from https://agupubs.onlinelibrary.wiley.com/doi/10.1029/2021JC018374 by Utrecht University Library, Wiley Online Library on [21/10/2022]. See the Terms and Conditions (https://onlinelibrary.wiley.com/terms-and-conditions) on Wiley Online Library for rules of use; OA articles are governed by the applicable Creative Commons License

Table 2
Wave Height and Bed Shear Stress Parameters Compared Between Present-Day and RCP8.5 Wave Climates for Two Shelf Sections, Without Morphologic Change

	Harrison Bay		Flaxman Island	
Wave Climate	Present-Day	RCP8.5	Present-day	RCP8.5
Avg H_s imposed at offshore boundary (m)	0.91	2.26	0.91	2.26
Avg T_p imposed at offshore boundary (p)	5.05	9.09	5.05	9.09
% Difference in H_s between present-day and RCP8.5 waves, from 80 to 0 m depth	N/A	114	N/A	134
% H_s attenuation between 80 and 10 m depth	37.5	53.7	14.5	23.2
Avg. inner shelf shear stresses, τ_{max} between 25 and 5 m depth (N/m^2)	0.56	1.66	0.97	2.90
Avg. depth of critical shear stress exceedance (m)	31.6	76.0	31.0	73.6
Avg. X-shelf distance of critical shear stress exceedance (km)	89.5	104	23.2	67.0
% Time critical shear stress exceedance for fine sand, 10 m isobath	52	100	50	100
% Time critical shear stress exceedance for fine sand, 40 m isobath	25	67	23	67
Maximum current speed at 25 m depth at 50 cm above bed (cm/s)	3.0	3.1	2.0	2.0

The critical shear stress for mobilization (τ_c) of the fine sands modeled in the seabed was approximately 0.23 N/m^2 for both shelf sections (Table 1). As a result of increased wave heights, the average water depth of τ_c exceedance on both shelves was approximately 31 m under present-day waves and 73–76 m under future RCP8.5 waves (Table 2). At Harrison Bay, the shelf break is located at approximately 25 m depth (88 km offshore), and thus fine sands were mobile across the entire shelf for both present and RCP8.5 waves (Table 2; Figure 5e). On the Flaxman Island section, fine sands were only mobile on the inner shelf (within 23.3 km of shore) for the present scenario, but this envelope expanded to encompass much of the shelf (66.9 km from shore) in the RCP8.5 scenario.

A stronger wave climate and lengthened open-water season increased the annual duration of shear stress exceedance for shelf sediments. This duration more than doubled across the entirety of the shelf for the more energetic RCP8.5 wave climate (Figures 5g and 5h). Portions of the inner shelf on each section became exposed to above-critical shear stresses for 100% of the year. Overall, the mobility of seabed sediment increased as both a function of greater wave height and period as well as a longer duration of exposure to wave orbital motion in the RCP8.5 wave climate.

Tidal forcings were minimal and remained constant in all model trials, and wind forcing was not included. Therefore, the only mechanisms for current-speed evolution through time were changes to water column depth through morphologic adjustment or barotropic flows driven by wave-setup. At Harrison Bay, maximum bottom current speeds measured at the 25 m isobath (50 cm above the seabed) were approximately 3 cm/s for both wave climates. At Flaxman Island, maxima were 2 cm/s at the 25 m isobath.

4.1.2. Sediment Transport Response

Wave-induced bed stresses led to greater sediment transport on the narrow and steep Flaxman Island transect than on the broad and flat Harrison Bay transect. Gradients in shear stresses across the shelf were controlled by the decay of wave heights and water depth (Figures 6a and 6b). As a result, cross-shelf gradients in suspended and bedload transport were dampened across Harrison Bay, but were substantial on the steep Flaxman Island section (Figures 6c and 6d). Transport direction also differed: net offshore transport occurred at Flaxman Island, while net onshore transport occurred at Harrison Bay.

Overall magnitudes of sediment transport (expressed as cumulative transport summed across the shelf for each 1000-year simulation) were greater for (a) the RCP8.5 wave climate and (b) Flaxman Island. Positive values indicate net onshore-directed transport driven by wave-orbital asymmetry, and negative values indicate downslope transport directed offshore. At Flaxman Island the principle mode of sediment transport was suspended load, which was two orders of magnitude greater than that of bedload. Suspended load increased ten-fold from

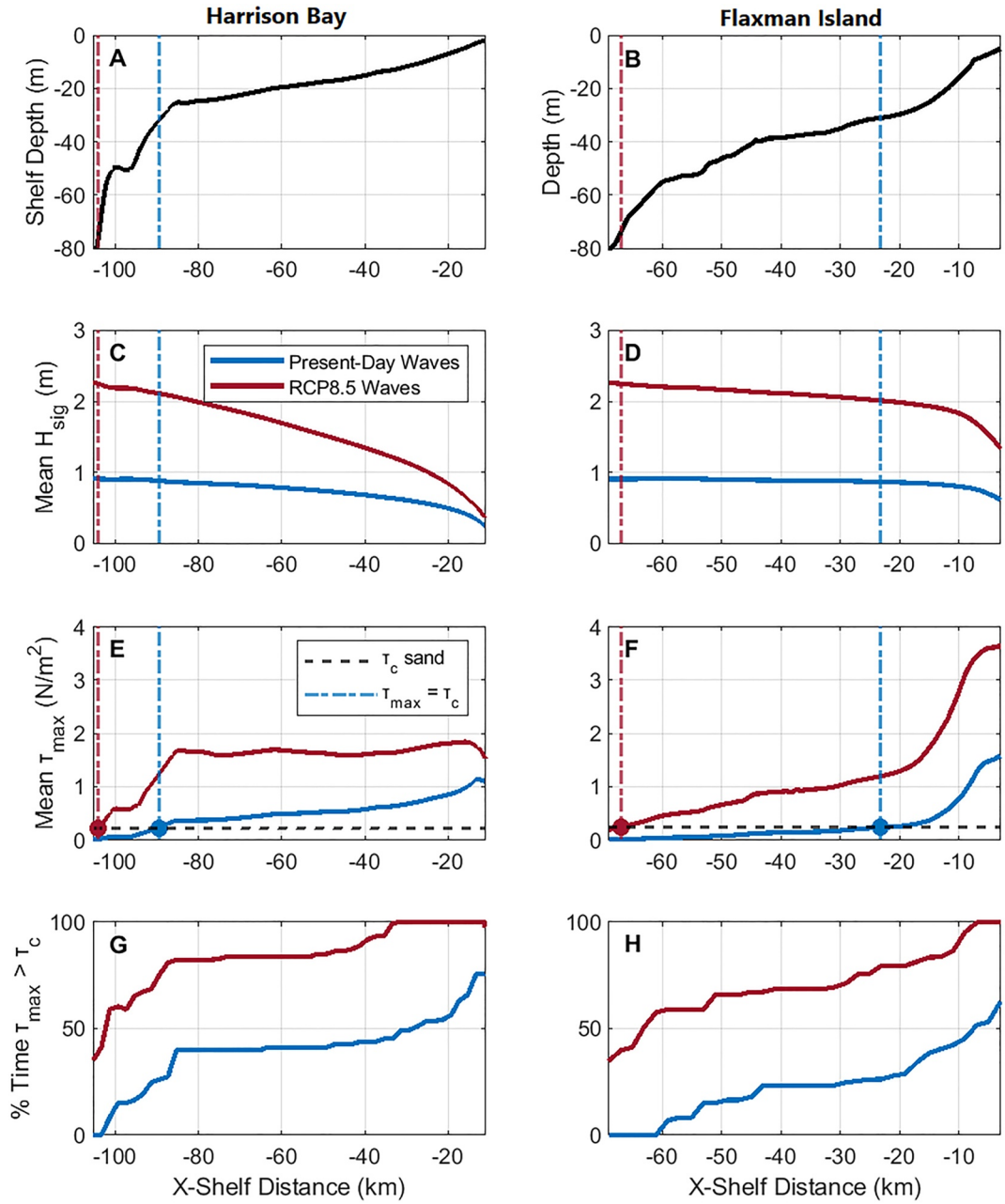

Figure 5. Wave heights and wave-induced shear stresses. (a and b) Initial cross-shelf sections are shown for Harrison Bay and Flaxman Island, respectively. (c and d) Average cross-shelf wave heights for the present-day and RCP8.5 wave climates. (e and f) Resultant temporally averaged wave-induced maximum bed shear stresses (τ_{max}) and critical shear stress for mobilization of fine sands (τ_c). (g and h) Percent duration of each 1000 year model run in which τ_c is exceeded. Vertical dashed lines show the outer depth of average sand mobilization in each wave climate.

-10.0×10^5 m^3/m in the present-day wave climate to -109×10^5 m^3/m in the RCP8.5 wave climate (Table 3). Suspended sediment transport was prevalent in a distinct morphodynamic envelope, whose seaward boundary increased from ~38 m depth under present-day waves to ~71 m depth under RCP8.5 waves (Figure 6d). Bedload transport increased from 0.311×10^5 m^3/m in the present-day wave climate to 0.651×10^5 m^3/m in the RCP8.5 wave climate, similarly expanding the seaward limit of transport from approximately 17 m depth under present-day waves to 27 m depth under RCP8.5 waves.

21699291, 2022, 9, Downloaded from https://agupubs.onlinelibrary.wiley.com/doi/10.1029/2021JC018374 by Utrecht University Library, Wiley Online Library on [21/10/2022]. See the Terms and Conditions (https://onlinelibrary.wiley.com/terms-and-conditions) on Wiley Online Library for rules of use; OA articles are governed by the applicable Creative Commons License

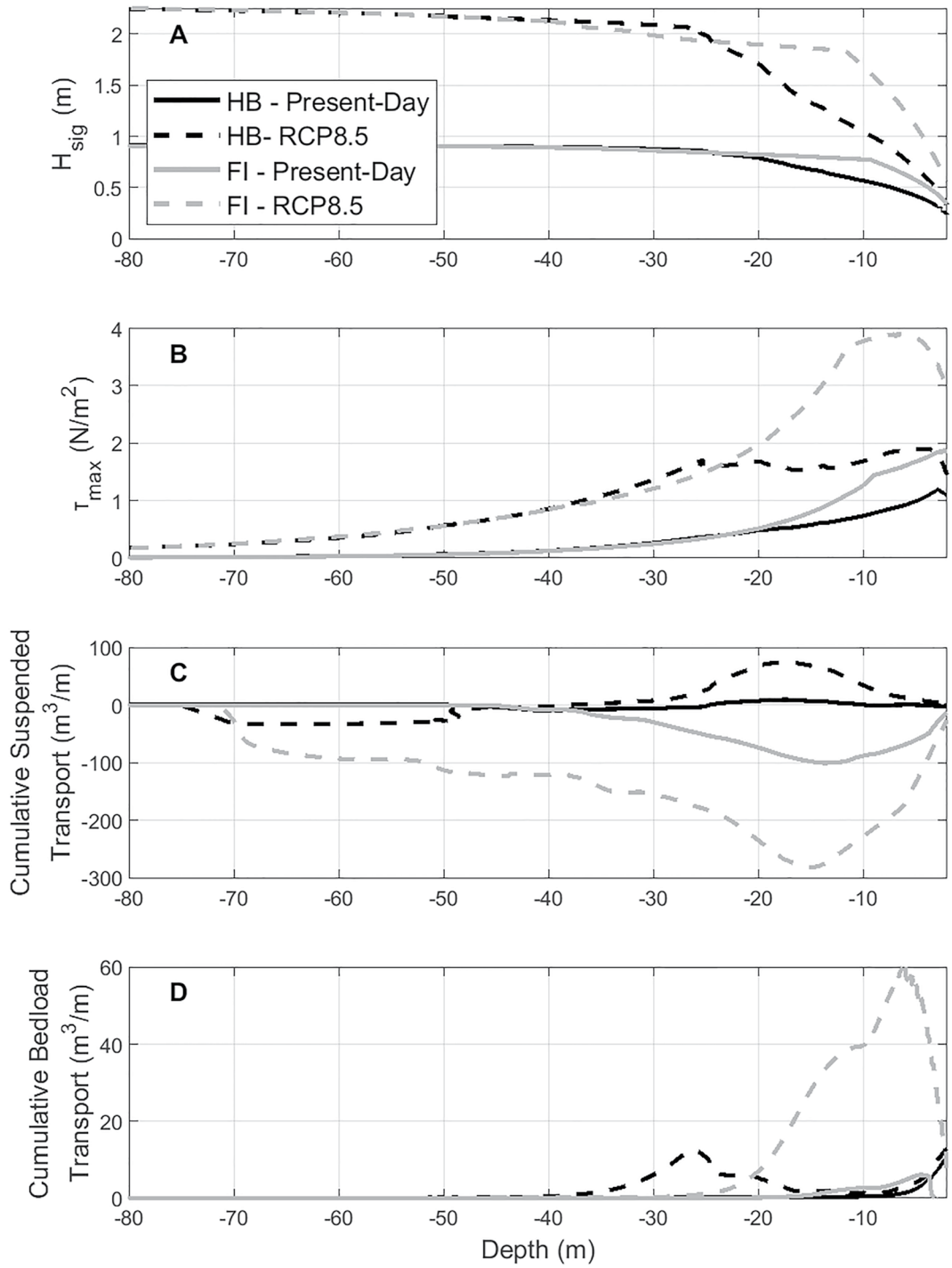

Figure 6. Contrasting gradients in sediment transport forcings, (a) average H_s and (b) bed shear stress resulting in contrasting suspended load and (c and d) bedload transport responses. Harrison Bay and Flaxman Island are shown as black and gray lines, respectively, and present-day and RCP8.5 waves are solid and dotted lines, respectively.

Transport at Harrison Bay increased an order of magnitude between the wave climates, from 0.761×10^5 m^3/m bedload and 1.99×10^5 m^3/m suspended load under the present-day wave climate to 4.16×10^5 m^3/m bedload and 30.2×10^5 m^3/m suspended load under the RCP8.5 wave climate (Table 3). The seaward boundary of onshore-directed bedload transport expanded from approximately 11 m in present-day waves to 40 m in RCP8.5

21699291, 2022, 9, Downloaded from https://agupubs.onlinelibrary.wiley.com/doi/10.1029/2021JC018374 by Utrecht University Library, Wiley Online Library on [21/10/2022]. See the Terms and Conditions (https://onlinelibrary.wiley.com/terms-and-conditions) on Wiley Online Library for rules of use; OA articles are governed by the applicable Creative Commons License

21699291, 2022, 9, Downloaded from https://agupubs.onlinelibrary.wiley.com/doi/10.1029/2021JC018374 by Utrecht University Library, Wiley Online Library on [21/10/2022]. See the Terms and Conditions (https://onlinelibrary.wiley.com/terms-and-conditions) on Wiley Online Library for rules of use; OA articles are governed by the applicable Creative Commons License

Table 3
Total Cumulative Sediment Transport and Final Mud Fractions Between the Inner and Middle Shelves of the Four Modeled Shelf Profiles

	Harrison Bay		Flaxman Island	
Wave Climate	Present-Day	RCP8.5	Present-Day	RCP8.5
Total volume of sediment transport				
Bedload (m^3/m)	0.761×10^5	4.16×10^5	0.311×10^5	6.51×10^5
Suspended load (m^3/m)	1.99×10^5	30.2×10^5	-10.0×10^5	-109×10^5
Mud fractions				
Initial fraction	0.71	0.71	0.88	0.88
Final avg. fraction 0–30 m depth	0.67	0.59	0.71	0.61
Final avg. fraction 30–60 m depth	0.49	0.22	0.94	0.94

Note. Negative transport totals indicate seaward sediment transport.

waves, and suspended load transport occurred in spatially varying zones across the shelf but was greater under RCP8.5 waves (Figures 6c and 6d).

Opposing directions of suspended load and bedload transport led to a cross-shelf gradient in grain size on the seabed which can provide insight to the fate of eroded sands and muds. On both shelf sections, RCP8.5 waves drove substantial textural changes, though with opposite patterns on the two transects. Initial sand/mud percentages were 29%/71% at Harrison Bay and 12%/88% at Flaxman Island. After 1000 years of RCP8.5 waves, the mud fraction in Harrison Bay between 30 and 60 m depth decreased from 71% to 22% (Table 3). Between 0 and 30 m depth winnowing was limited, and mud fractions decreased to from 71% to 59%.

In contrast, Flaxman Island experienced winnowing at shallower depths (0–30 m depth) and mud accumulation at greater depths (30–60 m depths), consistent with the seaward advection and diffusion of suspended load and re-deposition on the middle shelf (Table 3). This effect occurred under both present-day and RCP8.5 waves, but was amplified on the inner shelf in the RCP8.5 case, where mud fractions decreased from 88% initially to 71% and 61% under present-day and RCP8.5 waves, respectively. At greater depths, mud fractions increased 88%–94% in both wave climates due to deposition of eroded inner shelf muds (Table 3).

4.1.3. Morphologic Evolution

The majority of morphologic change occurred at depths shallower than 40 m. The general patterns of change after 1000 years were similar for both present-day and RCP8.5 simulations, but the RCP8.5 wave climate drove greater magnitudes of bed elevation changes and slope adjustment. On both shelves, an inflection point in bed elevation change represented a transition between zones of cross-shelf erosion and deposition. At Harrison Bay, this depth remained static at approximately 17 m for both wave climates, separating an area of slight erosion on the middle shelf from deposition on the inner shelf (Figures 7a and 7c). This indicated that the shelf profile is stable in time and space regardless of wave climate, because landward translation and changes to profile shape were minimal. However, at Flaxman Island the inflection point between inner shelf erosion and middle shelf deposition was 13.6 m in the present-day wave climate and 15.6 m in the RCP8.5 wave climate (Figures 7b and 7d), indicating that morphologic adjustment occurred to greater depths after exposure to a stronger wave climate.

Harrison Bay experienced relatively subtle morphologic changes overall. Erosion occurred near the shelf break, transitioning to deposition on the inner shelf (Figures 7a and 7c). For the present-day wave climate, an average of 11 cm of erosion occurred around the shelf break (between 40 and 17 m), in contrast to 3 cm of deposition over a broad distance from 17 m to the shoreline. For the RCP8.5 wave climate, an average of 42 cm of erosion occurred near the shelf break, and 47 cm of deposition between 17 m to the shoreline. Landward transport of sediments resulted in the emergence of an aggradational bar on the 2 m isobath. In addition to relatively minor adjustments to the profile shape, the profile did not undergo landward retreat.

In contrast, Flaxman Island experienced higher morphologic adjustment after exposure to both wave climates where erosion of the shoreline and inner shelf supplied deposition on the middle shelf (Figures 7b and 7d). After

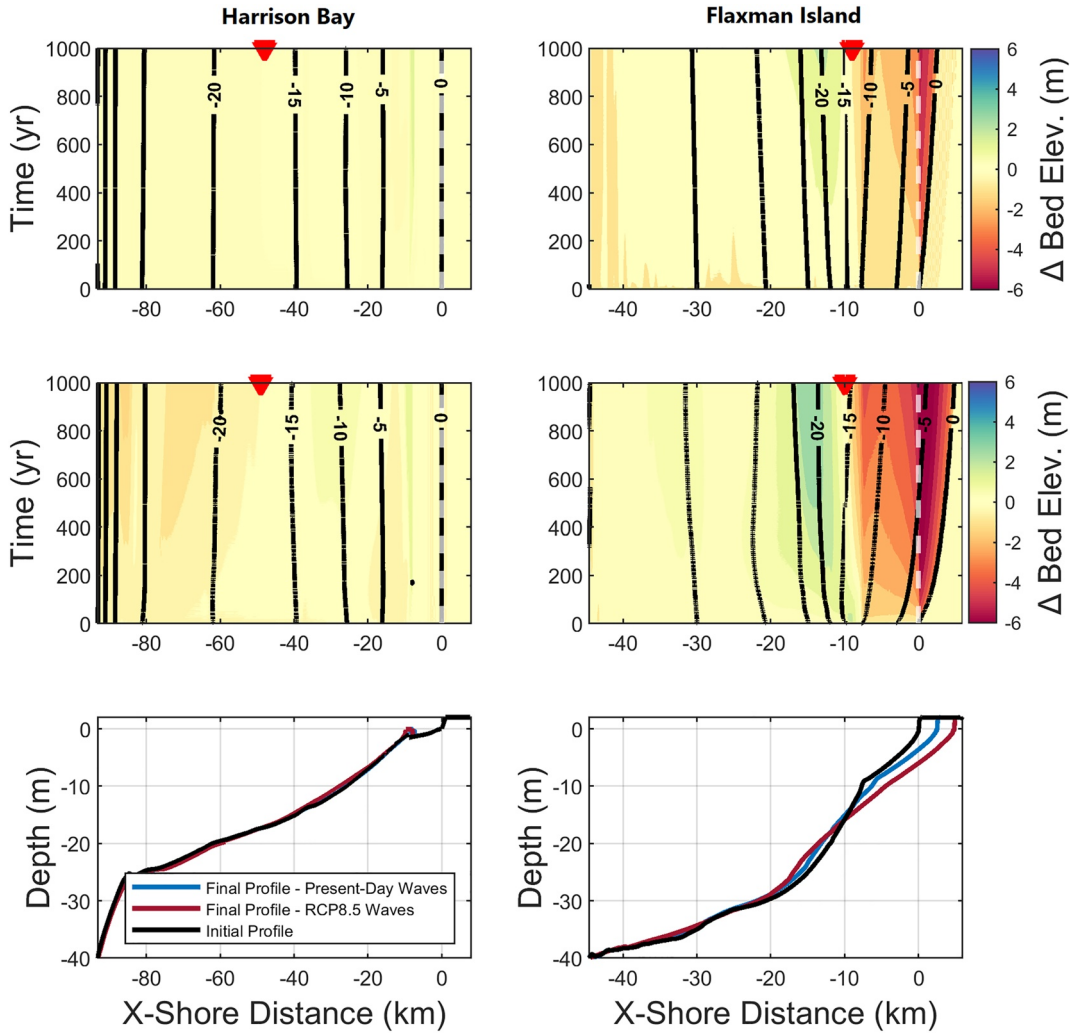

Figure 7. Changes in bed elevation through time. Panels (a and c) show morphologic response of Harrison Bay to present-day and RCP8.5 waves, respectively. Panels (b and d) show morphologic response of Flaxman Island to present-day and RCP8.5 waves, respectively. Contour lines are shown in black, and initial shoreline positions are shown by the white dashed line. Red triangles are the inflection points between erosion and deposition after 1000 years. Initial and final shelf cross sections are shown for (e) Harrison Bay and (f) Flaxman Island.

1000 years of exposure to present-day waves, an average of 1.47 m of erosion occurred between 13.7 m depth and the shoreline. Coastal sediments supplied from the inner shelf were deposited between 13.65 and 40 m depth, averaging 0.59 m of deposition. The RCP8.5 wave climate yielded bed level changes of the same character as the present-day wave climate, but of a greater magnitude. An average of 3.28 m of erosion occurred on the inner shelf between the shoreline and 15.88 m depth. Deposition on the middle shelf between 15.88 m depth and 40 m depth averaged 0.81 m.

4.1.4. Morphodynamic Feedbacks

Notable adjustments to the shelf profile at Flaxman Island enhanced the attenuation of waves propagating to the inner shelf, reducing wave heights at the coast. Decay in wave heights of 5.10% and 7.61% occurred at the 2 m isobaths after 1000 years of exposure to present-day and RCP8.5 waves, respectively (Figures 8b and 8d). Thus, eroded sediments conveyed to the middle shelf reduced wave heights reaching the inner shelf.

In contrast, wave heights generally remained constant through time at Harrison Bay in the present-day wave climate, with growth in height of up to 1.68% (at the 13 m isobath) and a decay up to 0.71% (at the 7 m isobath) (Figure 8a). In the RCP8.5 wave climate, wave heights grew up to 4.68% at the 13 m isobath where erosion

21699291, 2022, 9, Downloaded from https://agupubs.onlinelibrary.wiley.com/doi/10.1029/2021JC018374 by Utrecht University Library, Wiley Online Library on [21/10/2022]. See the Terms and Conditions (https://onlinelibrary.wiley.com/terms-and-conditions) on Wiley Online Library for rules of use; OA articles are governed by the applicable Creative Commons License

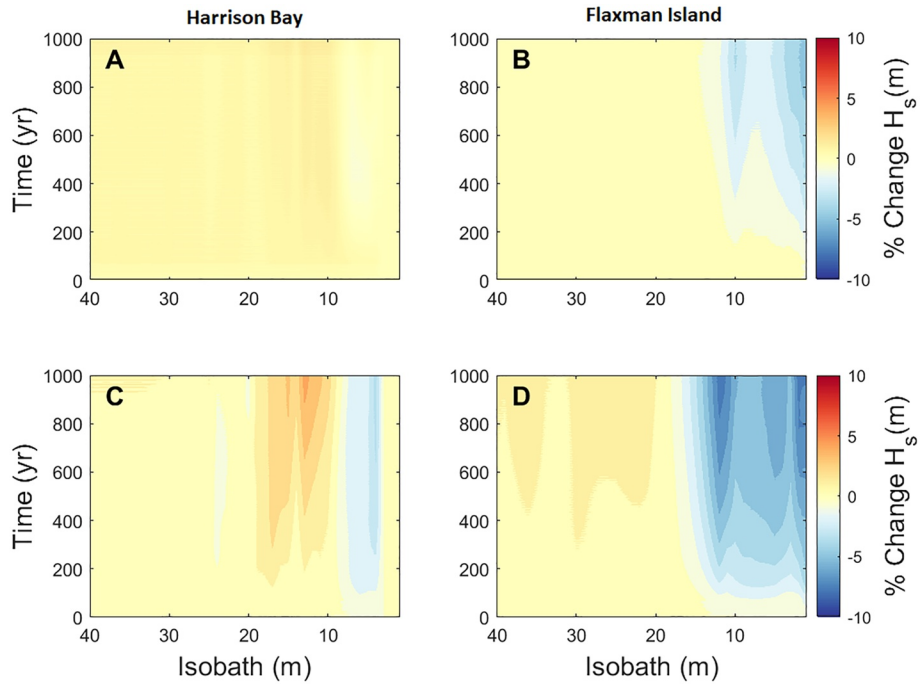

Figure 8. Changes in H_s through time driven by morphologic change expressed as a percent change from the initial yearly average. Panels (a and c) show H_s changes of Harrison Bay to present-day and RCP8.5 waves, respectively. Panels (b and d) show morphologic response of Flaxman Island to present-day and RCP8.5 waves, respectively.

occurred and waves decayed to 3.5% at the 4 m isobath where sediments were deposited on the inner shelf (Figure 8c). As a result of minimal morphologic change, Harrison Bay was relatively insulated from changes to wave heights which limited the potential for a morphodynamic feedback.

4.2. Storm Dynamics

Modeled wave heights and resultant shear stresses induced by storm waves were evaluated at the 10 m isobath to explore attenuation of storm waves prior to reaching the inner shelf. Since the same storm was applied to shelf profiles of different shapes, differences in modeled results are attributed to differences in wave attenuation across the shelf.

The delivery of waves to the inner shelf and resultant potential for sediment transport was once again controlled by the existing shelf morphology. Effective attenuation of waves on the flatter Harrison Bay sections led to significant wave heights of 0.60 and 0.61 m at the 10 m isobath on the present-day and RCP8.5 equilibrium shelf profiles, respectively. At Flaxman Island, the same storm generated wave heights of 0.74 m for both present-day and RCP8.5 cases (Table 4). As a result, the potential for sediment transport on the inner shelf was greater for Flaxman Island. Average bed shear stresses on the 10 m isobath at Flaxman Island were 1.19 and 1.16 N/m^2 on the present-day and RCP8.5-wave equilibrium profiles (Table 4). Thus, attenuation of waves passing over the

Table 4
Modeled Hydrodynamic and Sediment Transport Results From a Representative Arctic Storm Applied to the Four Output Shelf Profiles Generated in the Long-Term Evolution Simulations

	Harrison Bay		Flaxman Island	
Equilibrium profile	Present-day	RCP8.5	Present-day	RCP8.5
Avg. H_s (m) at 10 m depth	0.60	0.61	0.74	0.74
Cum. wave power at 10 m depth (kW/m)	8.43×10^6	8.70×10^6	13.9×10^6	13.5×10^6
Avg τ_{max} (N/m^2)	0.85	0.89	1.18	1.16

21699291, 2022, 9, Downloaded from https://agupubs.onlinelibrary.wiley.com/doi/10.1029/2021JC018374 by Utrecht University Library, Wiley Online Library on [21/10/2022]. See the Terms and Conditions (https://onlinelibrary.wiley.com/terms-and-conditions) on Wiley Online Library for rules of use; OA articles are governed by the applicable Creative Commons License

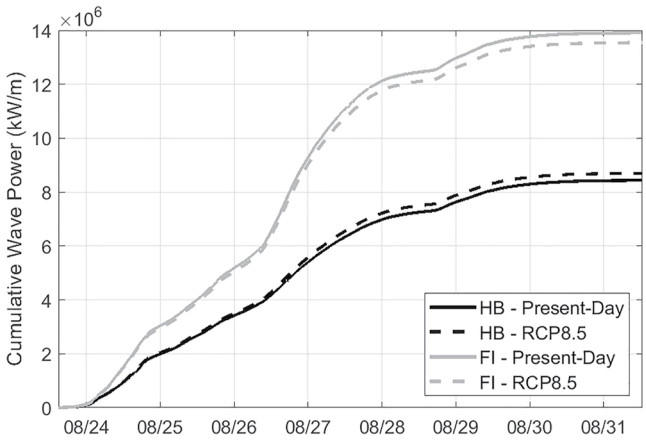

Figure 9. Cumulative wave power through the duration of the Arctic storm applied to the Harrison Bay (HB) and Flaxman Island (FI) equilibrium shelf profiles for current (solid) and future (dotted), computed at the 10 m isobath.

middle and outer shelf exerts a control on the potential for sediment resuspension and transport on the inner shelf.

Wave power on the inner portion of an Arctic shelf has been shown to scale with coastal erosion during storm events (Hequette & Barnes, 1990). Cumulative wave power at the 10 m isobath was calculated in this study using the shallow-water wave power equations outlined by Defne et al. (2009) and Fenton (1988). We find that the broad, gently sloping section at Harrison Bay mitigated the delivery of storm waves to the inner shelf more effectively than the steeper Flaxman Island section. The cumulative wave power at the 10 m isobath at Harrison Bay was 8.43×10^6 (kW/m) and 8.70×10^6 (kW/m) for the present-day and RCP8.5 equilibrium shelf profiles, respectively. At Flaxman Island, the same storm produced a cumulative wave power of 13.9×10^6 (kW/m) and 13.5×10^6 (kW/m) for the present-day and RCP8.5 equilibrium shelf profiles, respectively (values nearly twice that of Harrison Bay, Table 4).

As shown in Figure 9, wave power at Harrison Bay was consistently subdued relative to the Flaxman Island section as a result of the attenuation of peak storm waves prior to reaching the inner shelf. Furthermore, the Flaxman Island section evolved under RCP8.5 waves was shown to be slightly more insulated from storm waves than the present-day Flaxman Island section (Table 4) because the middle shelf had shallower depths and thus attenuated waves more effectively.

5. Discussion

As the influence of sea ice on Arctic shelf processes decreases under a warming climate, sediment transport will become increasingly dominated by open-water processes typical of shelves in temperate climates. A projected expansion in fetch due to reduced sea ice is expected to generate a more intense wave climate, and thus greater shear stresses on the seabed. These changes likely drive morphologic adjustment of Arctic continental shelves, beyond the existing adjustment expected in response to sea-level trends following the Last Glacial Maximum. This modeling study has demonstrated that relative magnitudes of morphologic adjustment are greater for (a) shelves of steeper slopes and (b) a projected future wave climate. A broad, gently sloping shelf (Harrison Bay) was relatively insulated from morphologic adjustment in both present-day and RCP8.5 wave climates due to effective cross-shelf attenuation of waves. In contrast, a narrower and steeper shelf (Flaxman Island) was more sensitive to enhanced wave heights and resultant bed shear stresses, which led to greater magnitudes of morphologic change. Furthermore, re-distribution of sediments from the inner shelf to the middle shelf created a feedback between morphologic change and wave attenuation, regulating climate-driven increases to wave heights on a relatively steep shelf.

5.1. Wave Attenuation in a Growing Wave Climate

Sea states in the Arctic are presently fetch-limited, both by ocean basin shape and the presence of pack ice (Casas-Prat & Wang, 2020). The resultant sea state during the open-water season is comparable in magnitude to the Gulf of Mexico (Stopa et al., 2016), but is expected to intensify (Casas-Prat & Wang, 2020; Thomson et al., 2016). Larger waves will interact with the seabed to greater depths, increasing the zone of potential sediment transport and the cross-shelf distance at which bottom friction can act to dissipate waves (e.g., Pruszak et al., 2008). As a result, climate-driven increases to the Arctic wave climate can manifest differently on shelves of different geometries.

Our modeled wave attenuation at Harrison Bay demonstrated that wave base encompassed a broad portion of the shelf, leading to substantial decay of waves propagating toward the coast. Figures 5c and 5d illustrates the gradual attenuation of both present-day and RCP8.5 waves across long distances at Harrison Bay, in contrast to minimal attenuation of waves across the shelf at Flaxman Island. This is consistent with observations of wave energy dissipation across shelves where bottom friction induced the seabed reduced the energy of waves passing over the shelf (Ardhuin et al., 2003; Gon et al., 2020; Palanques et al., 2002). In the Arctic, shelf sections along the Beaufort,

21699291, 2022, 9, Downloaded from https://agupubs.onlinelibrary.wiley.com/doi/10.1029/2021JC018374 by Utrecht University Library, Wiley Online Library on [21/10/2022]. See the Terms and Conditions (https://onlinelibrary.wiley.com/terms-and-conditions) on Wiley Online Library for rules of use; OA articles are governed by the applicable Creative Commons License

21699291, 2022, 9, Downloaded from https://agupubs.onlinelibrary.wiley.com/doi/10.1029/2021JC018374 by Utrecht University Library, Wiley Online Library on [21/10/2022]. See the Terms and Conditions (https://onlinelibrary.wiley.com/terms-and-conditions) on Wiley Online Library for rules of use; OA articles are governed by the applicable Creative Commons License

Chukchi, Laptev,and East Siberian seas tend to have broad widths and low relief (P. T. Harris et al., 2014), suggesting that effective damping of waves can insulate the inner shelf from both climate-driven wave growth and resultant morphologic change. Both modeled shelf sections were prescribed the same present-day and RCP8.5 wave climates, but experienced different magnitudes of wave-induced bed shear stresses on the inner shelf due to contrasting wave attenuation across the shelf. For example, between depths of 25 and 5 m, maximum bed shear stresses averaged over 1000 years of exposure to RCP8.5 waves were 1.66 (N/m^2) at Harrison Bay and 2.90 (N/m^2) at Flaxman Island (Table 2). Thus, the flatter shelf profile was more effective at reducing the impact of the intensified RCP8.5 wave climate on the seabed by attenuating waves across the shelf before they reached shallower depths. Because of this, the potential for wave-driven sediment transport and morphologic response at Harrison Bay was less than for Flaxman Island.

However, the character of morphologic response also depends on whether the changing wave climate is manifest more during extreme storm events or distributed evenly throughout the open-water season (see Ruggiero et al., 2010). In the Arctic, expected wave growth is a result of elongated fetch throughout the year, a dynamic long-term change (Smith & Thomson, 2016), but the expansion of open-water season into the stormy fall season increases exposure to episodic storm waves (Barnhart et al., 2014). This may impact the balance between morphologic disturbances by extreme storm events and fair-weather recovery of the shelf profile (Anderson et al., 2010; Farquharson et al., 2018; Ruggiero et al., 2016), with wave impacts dependent on initial shelf geometry. Thus, long-term predictions for morphologic responses may require a model with a temporal resolution that allows for both the influence of gradual fetch-driven increases to wave heights and increased storm exposure to be considered when projecting changes to the Arctic wave climate.

5.2. Morphologic Evolution and Feedbacks

An enhanced wave climate expanded the depth to which sediments were mobilized by waves, broadening the cross-shelf envelope of potential sediment disturbance and morphologic change on both shelves. Notably, morphologic adjustments were minimal at Harrison Bay as the shelf profile remained mostly stable and did not undergo landward retreat, while the Flaxman Island shelf section experienced alterations to the profile shape and retreat. Larger magnitudes and a more pronounced cross-shelf gradient of excess shear stresses on the steeper shelf section (Flaxman Island) led to greater morphologic change to greater depths on the shelf (Figure 5). After 1000 years of exposure to both present-day and RCP8.5 wave climates, Flaxman Island experienced an average of 1.47 m of vertical erosion on the inner shelf for present-day waves and 3.68 m of vertical erosion for RCP8.5 waves (Figure 7). Sediments eroded by waves from the inner shelf were conveyed downslope to a zone of reduced shear stresses at greater depths, leading to deposition on the middle shelf between 15 and 30 m depth. This redistribution of sediments accentuated the concave-upward shape of the inner shelf profile. The inflection point between inner shelf erosion and middle shelf deposition also deepened from 13.6 m depth in present-day waves to 15.6 m in the RCP8.5 wave climate, indicating that inner shelf erosion occurred to greater depths and that there was a greater change in shape of the shelf profile through time. On other shelves, stronger waves have been observed to drive sediment transport at greater depths, distributing sediments from zones of erosion on the inner shelf to the middle and outer shelf (Diesing et al., 2006; Forest et al., 2016; Guillén et al., 2006), consistent with the deepened zones of morphologic change modeled at Flaxman Island under RCP8.5 waves.

Rates of landward translation of the shelf profile also scaled with the input wave climate (Figures 7b and 7d). This morphologic adjustment to intensified waves was rapid initially but slowed through time, indicating the establishment of a morphodynamic equilibrium shelf profile set by the balance between wave climate, shoreface slope, and sediment textures (Friedrichs & Wright, 2004; Ortiz & Ashton, 2016). Thus, the steeper shelf section was more sensitive to the climate-driven growth in wave climate in terms of wave-induced erosion and landward profile translation, but sensitivity decreased as the shelf profile evolved and stabilized.

In contrast, weak gradients in bed stresses and sediment fluxes on the flat shelf section (Harrison Bay) limited cross-shelf exchange of sediment and resultant morphologic change (Figures 6, 7a, and 7c). Bed level changes across all areas of the shelf were <1 m in both wave climates (Figures 7a and 7c). Since the shape and position of the Harrison Bay profile remained relatively static in time and space under both wave climates, the gently sloping profile was thus closer to a state of morphodynamic equilibrium.

21699291, 2022, 9, Downloaded from https://agupubs.onlinelibrary.wiley.com/doi/10.1029/2021JC018374 by Utrecht University Library, Wiley Online Library on [21/10/2022]. See the Terms and Conditions (https://onlinelibrary.wiley.com/terms-and-conditions) on Wiley Online Library for rules of use; OA articles are governed by the applicable Creative Commons License

Redistribution of sediments on the steeper Flaxman Island section led to a regulatory morphodynamic feedback loop. Eroded coastal and inner shelf sediments were deposited in a stress-refuge on the middle shelf, leading to shallowing of the shelf profile and enhanced attenuation of waves propagating to the inner shelf and coast. Wave heights decayed 5.10% and 7.61% at the 2 m isobath as a result of 1000 years of morphologic evolution in the present-day and RCP8.5 wave climates, respectively (Figures 8b and 8d). This attenuation of waves slowed inner shelf erosion and mitigated the climate-driven increase to waves as the shelf profile evolved. Adjustments to Arctic shelf profiles have the potential to alter the character of waves that propagate to the inner shelf, promoting equilibration of the shelf profile. Furthermore, winnowing of fine-grained sediments in zones of high wave-induced bed stresses on the inner shelf left a surficial layer of coarser sediments that sheltered layers below from the wave boundary layer, armoring the seabed (Wiberg et al., 1994). Since the seabed of the ABS presently has patchy and diverse seabed textures as a result of ice gouging processes (Barnes et al., 1980), reduced sea ice and increased wave energy in the future may result in bed armoring that increases resistance of the inner shelf seabed to erosion (C. K. Harris & Wiberg, 2002; Thieler et al., 1995). This represents another potential mechanism for regulating erosion of inner shelf profiles, because Arctic coasts with coarser sediments have been found to be more resistant to erosion than other coastal morphotypes (Farquharson et al., 2018).

5.3. Implications

Arctic continental shelves are a key transition zone in which deep water waves are attenuated as they propagate to the coast. The geometry of the shelf, which can vary in time and space, impacts how a change in wave climate (i.e., due to a warming Arctic) manifests at the adjacent coastline. For example, the propagation of wave energy was modest across a lower-gradient shelf (Harrison Bay) relative to a higher-gradient shelf (Flaxman Island transect). This means lower-gradient shelf systems may experience reduced impacts on cross-shelf sediment transfer under a growing wave climate, and in turn experience smaller impacts on coastal erosion - at least in terms of mechanical erosion accomplished by breaking waves. Because thermal erosion is also important to the retreat of permafrost-rich bluffs (e.g., Obu et al., 2017), the retreat rate of shorelines like those backing Harrison Bay may see greater impacts from warming water temperatures than from an intensification of wave energy.

In contrast, the steeper section modeled at Flaxman Island exemplifies a steeper shelf which is more effective at conveying wave energy to the coast (resulting in greater coastal retreat). However, this section experiences a feedback cycle of sediment re-deposition on the middle shelf which actually buffers the sensitivity of the coast to these larger waves - and which can result in *reduced* nearshore wave energy for the same-sized storm imposed on the RCP8.5 versus present-day shelf profile (Figure 9). When predicting changes in coastal retreat as a function of changes in wave energy over centennial to millennial timescales, it is thus important to consider the geometry of the continental shelf and feedbacks between coastal erosion and re-deposition of coastal-sourced sediments on the shelf.

In this two-dimensional model, cross-shelf sediment conveyance was emphasized. In real shelf systems, along-shelf fluxes are typically an order of magnitude higher than cross-shelf fluxes, but have weaker gradients that reduce their relative impact on morphologic evolution (C. K. Harris & Wiberg, 2002; Palanques et al., 2002). Thus, the results here emphasize the trends in morphologic evolution that may occur on shelves of different geometries—but it is worth noting that an increase in height and/or period of the shore-oblique waves characteristic in this region (e.g., Weingartner et al., 2009) may drive a larger component of along-shelf sediment transfer in the future, especially on low-gradient shelves like Harrison Bay (where cross-shelf sediment transfer is already limited). In the model realm, this effect would amplify the results seen here, namely that morphologic feedbacks (in a cross-shelf view) are weak in the relatively low-gradient Harrison Bay.

While the continental shelf geometry has a demonstrable effect on variability in coastal processes, other factors are also expected to cause variability in shelf and shoreline dynamics. For example, variable ice content and sediment types in the bluffs can contribute to varying retreat rates (Farquharson et al., 2018; Harper, 1990; Hequette & Barnes, 1990), with implications for how much sediment is supplied to the inner shelf—and thus how much morphodynamic adjustment may occur (which in turn regulates wave energy). The emergence of an increased Arctic wave climate may vary in space and time, impacting coastal evolution unevenly. Seasonal shorefast ice also varies in space and time (Hošeková et al., 2020; Overeem et al., 2011), and barrier islands occur along some sections of the coast (Gibbs & Richmond, 2017), with implications for how much wave energy reaches the coast and what type of coastal deposit is being eroded. Predicted increases in riverine sediment supply (Overeem &

21699291, 2022, 9, Downloaded from https://agupubs.onlinelibrary.wiley.com/doi/10.1029/2021JC018374 by Utrecht University Library, Wiley Online Library on [21/10/2022]. See the Terms and Conditions (https://onlinelibrary.wiley.com/terms-and-conditions) on Wiley Online Library for rules of use; OA articles are governed by the applicable Creative Commons License

Syvitski, 2010) will make more sediment available to nearshore environments, which may also impact shelf evolution in locations near rivers (see Fagherazzi & Overeem, 2007; Friedrichs & Wright, 2004). Future sea-level rise may also impact shelf and shoreline dynamics, though the present regional rate is 3.5 ± 1 mm/yr (Couture et al., 2018; Erikson et al., 2020), whereas changes to significant wave height in the Arctic are on the order of cm/yr (Casas-Prat & Wang, 2020; Wang et al., 2015). Changes in wave height thus may have a more substantial effect on coastal evolution (e.g., Ruggiero, 2013), amplifying the need for a thorough understanding of morphodynamic feedbacks on the cross-shelf transfer of wave energy to the coast.

6. Conclusion

This study presents modeled impacts of climate-driven wave growth on the morphology of the Alaskan Beaufort Shelf (at centennial to millennial timescales), as well as morphodynamic feedbacks which may regulate wave energy reaching the coast. These findings are relevant for understanding the long-term vulnerability of Arctic coastal communities and infrastructure due to marine forcings and resultant coastal erosion.

We found that the morphologic response of the continental shelf to a growing wave climate was controlled by initial shelf slope geometry. On a steeper shelf section (Flaxman Island, AK), project future waves (based on emissions scenario RCP8.5) led to enhanced cross-shelf gradients in wave-induced bed stresses and sediment fluxes. Morphologic change was characterized by distinct zones of erosion on the inner shelf (between 0 and 16 m depth) and deposition on the middle shelf (between 16 and 30 m depth), as sediments supplied by the eroding inner shelf profile were transported downslope to a zone of relaxed bed shear stresses. Deposition on the middle shelf led to effective dissipation of waves through time, ultimately reducing the height of waves reaching the 2 m isobath by 7.61% over 1000 years of morphologic adjustment. This represents a regulatory morphodynamic feedback in which climate-driven wave growth was mitigated by alterations to the shelf profile, particularly by wave attenuation over the shallower middle shelf. In contrast, a wide, lower-gradient shelf section (Harrison Bay, AK) was more effective at attenuating waves propagating across the shelf, thus insulating the inner shelf from both present-day and RCP8.5 waves and limiting morphologic adjustment and landward shoreline retreat. Since waves were attenuated over a broader cross-shelf distance on the flatter shelf section, cross-shelf gradients in bed stresses were small, resulting in limited cross-shelf transport and morphologic change. Furthermore, we found that storm waves (as in the case of fairweather waves) were more effectively attenuated across the shallow, low-gradient Harrison Bay shelf. However, morphologic adjustment of the steeper, more wave-sensitive Flaxman Island section under RCP8.5 fairweather waves resulted in better attenuation of storm waves than in the present case.

The findings of this study illustrate the importance of considering shelf profile geometry and sediment transport processes when evaluating morphologic changes to Arctic shelves and shorelines in a warming climate. This framework can provide insight to shelf environments beyond the Arctic, in which a shift in wave climate can drive differing sediment transport and morphologic responses depending on the initial cross-shelf geometry.

Appendix A

A1. Sensitivity Test for Morphologic Scaling Factor

A Brier Skill Score (BSS) was used to determine the highest *MF* value in which morphologic change could be computed over 1000 years with the minimum computation time, following the methods outlined by Ranasinghe et al. (2011).

$$BSS = 1 - \frac{(z_b - z_{b,mf1})^2}{(z_1 - z_{b,mf1})^2} \tag{A1}$$

where z_1 is the initial bed slope, z_b is the final bed slope with MF > 1, and $z_{b,mf1}$ is the final bed slope for a baseline trial in which MF = 10. Present-day waves were applied to the shelf profiles under combinations of flow simulation time and MF values (ranging from the baseline value of 10 incrementally up to 500) which represented 1000 years of morphologic change. The results of the sensitivity test showed that an MF of 100 could be used to reliably evaluate morphologic change.

21699291, 2022, 9, Downloaded from https://agupubs.onlinelibrary.wiley.com/doi/10.1029/2021JC018374 by Utrecht University Library, Wiley Online Library on [21/10/2022]. See the Terms and Conditions (https://onlinelibrary.wiley.com/terms-and-conditions) on Wiley Online Library for rules of use; OA articles are governed by the applicable Creative Commons License

A2. Active Sediment Layer Thickness

The thickness of the top seabed layer, or active layer, was set to 20 cm based on the formulation proposed by Warner et al. (2008):

$$z_a = \max\left[k_1\left(\tau_{sf} - \bar{\tau_{ce}}\rho_0, 0\right] + k_2 d_{50}\right. \quad \text{(A2)}$$

where τ_{sf} is the maximum skin friction stress from combined waves and currents, τ_{ce} is the critical shear stress for erosion, ρ_0 is the surface seawater density, d_{50} is the median seabed grain diameter, and k_1 and k_2 are constants 0.007 and 6.0, respectively. Below the top layer, the seabed was split into four layers with thicknesses increasing with depth so that the total seabed thickness was 10 m.

A3. Additional Model Parameters

Table A1 provides a supplemental overview of sediment transport and hydrodynamic model parameters implemented in Delft3D-FLOW.

A4. Model Limitations

It is worth noting several processes not incorporated in this model, in order to provide insight for future efforts. First, the model does not include along-shore components of forcing mechanisms, predicated on the idea that cross-shore gradients in bed stresses and sediment transport are stronger than along-shelf gradients and thus contribute more to cross-shelf morphology. That being said, a depth-averaged two-dimensional planview model or full three-dimensional model would be instructive for assessing impacts of shore-oblique waves, shore-oblique winds, and shelf steering of currents. Second, the model does not address sea ice, but rather focuses on the open-water season which is expected to encompass 365 days per year by the next century (see references in main text). But presently, sea ice bulldozes sediments locally and may entrain and raft sediments, representing mixing and advection terms, respectively. These terms have been historically unconstrained quantitatively but are interesting to consider. Third, the model does not incorporate spatially varying bed erodibility, which should be important because of ice keel scouring. A revised version of the model is in production which addresses ice-impacted bed erodibility. Fourth, the model does not address changing sediment supplies from accelerated coastal erosion or changes in river dynamics. Nor does it address variably grain size and ice content in the bluffs. A new version of the model is being tested using variable river supply. Bluff dynamics offer an important target

Table A1
Supplemental Overview of Sediment Transport and Hydrodynamic Model Parameters Implemented in Delft3D-FLOW

Parameter	Description	Value
Sediment Transport		
Morfac	Morphologic scaling factor	100
Ks	Bed roughness height influenced by skin friction and form drag	0.02
AlfaBs	Streamwise bed-gradient factor for bedload transport	1
AlfaBn	Transverse bed-gradient factor for bedload transport	1.5
SUSc	Current-related suspended sediment transport parameter	0.8
SUSw	Wave-related suspended sediment transport parameter	0.2
BEDc	Current-related bedload sediment transport parameter	1
BEDw	Wave-related bedload sediment transport parameter	0.2
BEDw	Wave-related bedload sediment transport parameter	0.2
Hydrodynamics		
Flam	Wave breaker delay parameter	2
Gamdis	Wave height to water depth ratio imposes wave breaking	0.5
FwFac	Streaming effect in wave boundary layer, typically set to zero	0
Betarol	Slope of wavefront	0.03

for future work. Fifth, it is unknown if the present shelves are in equilibrium with waves, or if they are approaching an equilibrium following rapid and then slow sea-level rise after the Last Glacial Maximum. It is likely that the shelves are in disequilibrium. A Holocene-timescale model of shelf evolution would be of interest.

Data Availability Statement

ERA5 wave hindcast data are available at the Copernicus Data Hub (https://scihub.copernicus.eu/), supported by the European Space Agency. Wave mooring data from the Alaskan Beaufort Shelf are available from the data repository for the Coastal Ocean Dynamics in the Arctic (CODA) 2019 cruise (https://digital.lib.washington.edu/researchworks/handle/1773/47139). Bathymetric data were also collected aboard the CODA cruises in 2019 (https://doi.org/10.7284/908599) and 2020 (https://doi.Org/10.7284/908921). Model setup and output data files can be found in the Arctic Data Center at https://arcticdata.io/catalog/view/doi:10.18739/A2H70820F.

Acknowledgments
We sincerely thank Jim Thomson, the Coastal Ocean Dynamics in the Arctic research team, and the captain and crew of the R/V Sikuliaq for assistance with field data collection and interpretation. We also thank collaborators Nina Stark and Jeff Obelcz for their assistance in the project design, Li Erikson (USGS) for sharing gridded NOS sounding data for the inner Beaufort Shelf, and Brad Murray and an anonymous reviewer for their thoughtful comments on the manuscript. This project was funded by the US National Science Foundation under project OPP 1913195. Jaap Nienhuis acknowledges funding from NWO VI.Veni.192.123.

References

Anderson, T. R., Neil Frazer, L., & Fletcher, C. H. (2010). Transient and persistent shoreline change from a storm. *Geophysical Research Letters*, *37*(8), 1–5. https://doi.org/10.1029/2009GL042252

Ardhuin, F., O'Reilly, W. C., Herbers, T. H. C., & Jessen, P. F. (2003). Swell transformation across the continental shelf. Part I: Attenuation and directional broadening. *Journal of Physical Oceanography*, *33*(9), 1921–1939. https://doi.org/10.1175/1520-0485

Arp, C. D., Jones, B. M., Schmutz, J. A., Urban, F. E., & Jorgenson, M. T. (2010). Two mechanisms of aquatic and terrestrial habitat change along an Alaskan Arctic coastline. *Polar Biology*, *33*(12), 1629–1640. https://doi.org/10.1007/s00300-010-0800-5

Barnes, P. W., Asbury, J. L., Rearic, D. M., & Ross, C. R. (1987). Ice erosion of a sea-floor knickpoint at the inner edge of the stamukhi zone, Beaufort Sea, Alaska. *Marine geology*, *76*, 207–222. https://doi.org/10.1016/0025-3227(87)90030-2

Barnes, P. W., & Rearic, D. M. (1985). Rates of sediment disruption by sea ice as determined from characteristics of dated ice gouges created since 1975 on the inner shelf of the Beaufort Sea. *USGS Open-File Report, No. 85-463*.

Barnes, P. W., & Reimnitz, E. (1982). Net flow of near-bottom waters on the inner Beaufort Sea Shelf as determined from seabed drifters. *USGS Open-File Report, No. 85-463*.

Barnes, P. W., Reimnitz, E., & Ross, R. (1980). Nearshore surficial sediment textures, Beaufort Sea, Alaska. *USGS Open-File Report, No. 80-196*.

Barnhart, K. R., Miller, C. R., Overeem, I., & Kay, J. E. (2016). Mapping the future expansion of Arctic open water. *Nature Climate Change*, *6*(3), 280–285. https://doi.org/10.1038/nclimate2848

Barnhart, K. R., Overeem, I., & Anderson, R. S. (2014). The effect of changing sea ice on the physical vulnerability of Arctic coasts. *The Cryosphere*, *8*(5), 1777–1799. https://doi.org/10.5194/tc-8-1777-2014

Blanco-Chao, R., Costa-Casais, M., Cajade-Pascual, D., & Gómez-Rey, G. (2019). Coastal retreat and sedimentation during the last 3000 years. Atlantic coast of NW Spain. *Journal of Marine Science and Engineering*, *7*(10), 331. https://doi.org/10.3390/jmse7100331

Box, J. E., Colgan, W. T., Christensen, T. R., Schmidt, N. M., Lund, M., Parmentier, F. J. W., et al. (2019). Key indicators of Arctic climate change: 1971–2017. *Environmental Research Letters*, *14*(4), 045010. https://doi.org/10.1088/1748-9326/aafc1b

Casas-Prat, M., & Wang, X. L. (2020). Sea ice retreat contributes to projected increases in extreme Arctic Ocean surface waves. *Geophysical Research Letters*, *47*(15), e2020GL088100. https://doi.org/10.1029/2020G-L088100

Casas-Prat, M., Wang, X. L., & Swart, N. (2018). CMIP5-based global wave climate projections including the entire Arctic Ocean. *Ocean Modelling*, *123*, 66–85. https://doi.org/10.1016/j.-ocemod.2017.12.003

Couture, N. J., Irrgang, A., Pollard, W., Lantuit, H., & Fritz, M. (2018). Coastal erosion of permafrost soils along the Yukon Coastal Plain and fluxes of organic carbon to the Canadian Beaufort Sea. *Journal of Geophysical Research: Biogeosciences*, *123*(2), 406–422. https://doi.org/10.1002/2017JG004166

Day, J. J., Holland, M. M., & Hodges, K. I. (2018). Seasonal differences in the response of Arctic cyclones to climate change in CESM1. *Climate Dynamics*, *50*(9–10), 3885–3903. https://doi.org/10.1007/s00382-017-3767-x

Dean, R. G., & Dalrymple, R. A. (2004). *Coastal processes with engineering applications*. Cambridge University Press.

Defne, Z., Haas, K. A., & Fritz, H. M. (2009). Wave power potential along the Atlantic coast of the southeastern USA. *Renewable Energy*, *34*(10), 2197–2205. https://doi.org/10.1016/j.renene.2009.02-.019

Deltares (2014). *User Manual Delft3D*. Deltares.

Diesing, M., Kubicki, A., Winter, C., & Schwarzer, K. (2006). Decadal scale stability of sorted bedforms, German Bight, southeastern North Sea. *Continental Shelf Research*, *26*(8), 902–916. https://doi.org/10.1016/j.csr.2006.02.009

Dufois, F., Garreau, P., Le Hir, P., & Forget, P. (2008). Wave- and current-induced bottom shear stress distribution in the Gulf of Lions. *Continental Shelf Research*, *28*(15), 1920–1934. https://doi.org/10.1016/j.csr.2008.03.028

Erikson, L. H., Gibbs, A. E., Richmond, B. M., Storlazzi, C. D., Jones, B. M., & Ohman, K. A. (2020). Changing storm conditions in response to projected 21st century climate change and the potential impact on an Arctic Barrier Island – Lagoon system — A Pilot study for Arey Island and Lagoon, Eastern Arctic Alaska. *USGS Open-File Report, No. 2020-1142*.

Fagherazzi, S., & Overeem, I. (2007). Models of deltaic and inner continental shelf landform evolution. *Annual Review of Earth and Planetary Sciences*, *35*(1), 685–715. https://doi.org/10.1146/annurev-.earth.35.031306.140128

Farquharson, L. M., Mann, D. H., Swanson, D. K., Jones, B. M., Buzard, R. M., & Jordan, J. W. (2018). Temporal and spatial variability in coastline response to declining sea-ice in northwest Alaska. *Marine Geology*, *404*, 71–83. https://doi.org/10.1016/j.margeo.2018.07.007

Fenton, J. D. (1988). The numerical solution of steady water wave problems. *Computers and Geosciences*, *14*(3), 357–368. https://doi.org/10.1016/0098-3004(88)90066-0

Fischbein, S. A. (1987). Analysis and interpretation of ice-deformed sediments from Harrison Bay, Alaska. *USGS Open-File Report, No. 87-262*.

Forest, A., Osborne, P. D., Curtiss, G., & Lowings, M. G. (2016). Current surges and seabed erosion near the shelf break in the Canadian Beaufort Sea: A response to wind and ice motion stress. *Journal of Marine Systems*, *160*, 1–16. https://doi.org/10.1016/j.jmarsys.2016.03.008

Friedrichs, C. T., & Wright, L. D. (2004). Gravity-driven sediment transport on the continental shelf: Implications for equilibrium profiles near river mouths. *Coastal Engineering*, *51*(8–9), 795–811. https://doi.org/10.1016/j.coastaleng.2004.07.010

21699291, 2022, 9, Downloaded from https://agupubs.onlinelibrary.wiley.com/doi/10.1029/2021JC018374 by Utrecht University Library, Wiley Online Library on [21/10/2022]. See the Terms and Conditions (https://onlinelibrary.wiley.com/terms-and-conditions) on Wiley Online Library for rules of use; OA articles are governed by the applicable Creative Commons License

Gibbs, A. E., Harden, E. L., Richmond, B. M., & Erikson, L. H. (2011). Regional shoreline change and coastal erosion hazards in Arctic Alaska. In *Solutions to Coastal Disasters 2011* (pp. 258–272).

Gibbs, A. E., Nolan, M., & Richmond, B. M. (2015). Evaluating changes to arctic coastal bluffs using repeat aerial photography and structure from-motion elevation models. In *The Proceedings of the Coastal Sediments 2015*. https://doi.org/10.1142/97898146899770080

Gibbs, A. E., & Richmond, B. M. (2017). National assessment of shoreline change — Historical shoreline change along the north coast of Alaska, U.S. -Canadian border to Icy Cape. *U.S. Geological Survey Open File Report 2015 - 1048, 96*.

Gon, C. J., MacMahan, J. H., Thornton, E. B., & Denny, M. (2020). Wave dissipation by bottom friction on the inner shelf of a Rocky shore. *Journal of Geophysical Research: Oceans*, *125*(10), e2019JC015963. https://doi.org/10.1029/2019JC015963

Guillén, J., Bourrin, F., Palanques, A., De Madron, X. D., Puig, P., & Buscail, R. (2006). Sediment dynamics during wet and dry storm events on the Têt inner shelf (SW Gulf of Lions). *Marine Geology*, *234*(1–4), 129–142. https://doi.org/10.1016/j.margeo.2006.09.018

Harper, J. R. (1990). Morphology of the Canadian Beaufort Sea coast. *Marine Geology*, *91*(1–2), 75–91. https://doi.org/10.1016/0025-3227(90)90134-6

Harris, C. K., & Wiberg, P. (2002). Across-shelf sediment transport: Interactions between suspended sediment and bed sediment. *Journal of Geophysical Research*, *107*(C1), 3008. https://doi.org/10.1029/2000jc000634

Harris, P. T., & Macmillan-Lawler, M. (2016). Global overview of continental shelf geomorphology based on the SRTM30_PLUS 30-arc second database. *Coastal Research Library*, *13*, 169–190. https://doi.org/10.1007/978-3-319-25121-9_7

Harris, P. T., Macmillan-Lawler, M., Rupp, J., & Baker, E. K. (2014). Geomorphology of the oceans. *Marine Geology*, *352*, 4–24. https://doi.org/10.1016/j.margeo.2014.01.011

Hequette, A., & Barnes, P. W. (1990). Coastal retreat and shoreface profile variations in the Canadian Beaufort Sea. *Marine Geology*, *91*(1–2), 113–132. https://doi.org/10.1016/0025-3227(90)90136-8

Héquette, A., Desrosiers, M., & Barnes, P. W. (1995). Sea ice scouring on the inner shelf of the southeastern Canadian Beaufort Sea. *Marine Geology*, *128*(3–4), 201–219. https://doi.org/10.1016/0025-3227(95)00095-G

Héquette, A., Desrosiers, M., Hill, P. R., & Forbes, D. L. (2001). The influence of coastal morphology on shoreface sediment transport under storm-combined flows, Canadian Beaufort Sea. *Journal of Coastal Research*, *17*(3), 507–516.

Héquette, A., & Hill, P. R. (1993). Storm-generated currents and offshore sediment transport on a sandy shoreface, Tibjak Beach, Canadian Beaufort Sea. *Marine Geology*, *113*(3–4), 283–304. https://doi.org/10.1016/0025-3227(93)90023-O

Héquette, A., Ruz, M. H., & Hill, P. R. (1995b). The effects of the Holocene sea level rise on the evolution of the southeastern coast of the Canadian Beaufort Sea. *Journal of Coastal Research*, 494–507.

Hersbach, H., Bell, B., Berrisford, P., Biavati, G., Horányi, A., Muñoz Sabater, J., et al. (2018). *ERA5 hourly data on single levels from 1979 to present*. Copernicus Climate Change Service (C3S) Climate Data Store (CDS). https://doi.org/10.24381/cds.adbb2d47

Hill, P. R., Blasco, S. M., Harper, J. R., & Fissel, D. B. (1991). Sedimentation on the Canadian Beaufort shelf. *Continental Shelf Research*, *11*(8–10), 821–842. https://doi.org/10.1016/0278-4343(91)90081-g

Hill, P. R., Mudie, P. J., Moran, K., & Blasco, S. M. (1985). A sea-level curve for the Canadian Beaufort shelf. *Canadian Journal of Earth Sciences*, *22*(10), 1383–1393. https://doi.org/10.1139/e85-146

Hošeková, L., Malila, M. P., Rogers, W. E., Roach, L. A., Eidam, E., Rainville, L., et al. (2020). Attenuation of ocean surface waves in pancake and frazil sea ice along the coast of the Chukchi Sea. *Journal of Geophysical Research: Oceans*, *125*(12), e2020JC016746. https://doi.org/10.1029/2020J-C016746

Jakobsson, M., Mayer, L. A., Bringensparr, C., Castro, C. F., Mohammad, R., Johnson, P., et al. (2020). The international bathymetric chart of the Arctic Ocean version 4.0. *Scientific Data*, *7*(1), 176. https://doi.org/10.1038/s41597-020-0520-9

Kistler, R., Kalnay, E., Collins, W., Saha, S., White, G., Woollen, J., et al. (2001). The NCEP-NCAR 50-year reanalysis: Monthly means CD-ROM and documentation. *Bulletin of the American Meteorological Society*, *82*(2), 247–267. https://doi.org/10.1175/1520-0477(2001)082<0247:tnnyrm>2.3.co;2

Lacy, J. R., & MacVean, L. J. (2016). Wave attenuation in the shallows of San Francisco Bay. *Coastal Engineering*, *114*, 159–168. https://doi.org/10.1016/j.coastaleng.2016.03.008

Lesser, G. R., Roelvink, J. A., van Kester, J. A. T. M., & Stelling, G. S. (2004). Development and validation of a three-dimensional morphological model. *Coastal Engineering*, *51*(8–9), 883–915. https://doi.org/10.1016/j.coastaleng.2004.07.014

Lynch, A. H., Curry, J. A., Brunner, R. D., & Maslanik, J. A. (2004). Toward an integrated assessment of the impacts of extreme wind events on Barrow, Alaska. *Bulletin of the American Meteorological Society*, *85*(2), 209–222. https://doi.org/10.1175/bams-85-2-209

Manrique, D. R., Corral, S., & Guimarães Pereira, Â. (2018). Climate-related displacements of coastal communities in the Arctic: Engaging traditional knowledge in adaptation strategies and policies. *Environmental Science and Policy*, *85*, 90–100. https://doi.org/10.1016/j.envsci.2018.04-.007

Manson, G. K., & Solomon, S. M. (2007). Past and future forcing of Beaufort Sea coastal change. *Atmosphere-Ocean*, *45*(2), 107–122. https://doi.org/10.3137/ao.450204

National Atmospheric and Oceanic Administration (NOAA). (2022). Sea level trends. Retrieved from https://tidesandcurrents.noaa.gov/sltrends/sltrends.html

Nittrouer, C. A., & Wright, L. D. (1994). Transport of particles across continental shelves. *Reviews of Geophysics*, *32*(1), 85–113. https://doi.org/10.1029/93RG02603

Norton, D., & Weller, G. (1984). The Beaufort Sea: Background, history, and perspective. https://doi.org/10.1016/B978-0-12-079030-2.50007-1

Obu, J., Lantuit, H., Grosse, G., Günther, F., Sachs, T., Helm, V., & Fritz, M. (2017). Coastal erosion and mass wasting along the Canadian Beaufort Sea based on annual airborne LiDAR elevation data. *Geomorphology*, *293*, 331–346. https://doi.org/10.1016/j.geomorph.2016.02.014

Ogston, A. S., Cacchione, D. A., Sternberg, R. W., & Kineke, G. C. (2000). Observations of storm and river flood-driven sediment transport on the northern California continental shelf. *Continental Shelf Research*, *20*(16), 2141–2162. https://doi.org/10.1016/S0278-4343(00)00065-0

Ogston, A. S., & Sternberg, R. W. (1999). Sediment-transport events on the northern California continental shelf. *Marine Geology*, *154*(1–4), 69–82. https://doi.org/10.1016/S0025-3227(98)00104-2

Okkonen, S. R. (2016). *Sea level measurements along the Alaskan Chukchi and Beaufort coasts*. Coastal Marine Institute, University of Alaska Fairbanks.

Ortiz, A. C., & Ashton, A. D. (2016). Exploring shoreface dynamics and a mechanistic explanation for a morphodynamic depth of closure. *Journal of Geophysical Research: Earth Surface*, *121*(2), 442–464. https://doi.org/10.1002/2015JF003699

Overeem, I., Anderson, R. S., Wobus, C. W., Clow, G. D., Urban, F. E., & Matell, N. (2011). Sea ice loss enhances wave action at the Arctic coast. *Geophysical Research Letters*, *38*(17), 1–6. https://doi.org/10.1029/2011GL048681

Overeem, I., Nienhuis, J. H., & Piliouras, A. (2022). Ice-dominated Arctic deltas. *Nature Reviews Earth and Environment*, *3*(4), 225–240. https://doi.org/10.1038/s43017-022-00268-x

21699291, 2022, 9, Downloaded from https://agupubs.onlinelibrary.wiley.com/doi/10.1029/2021JC018374 by Utrecht University Library, Wiley Online Library on [21/10/2022]. See the Terms and Conditions (https://onlinelibrary.wiley.com/terms-and-conditions) on Wiley Online Library for rules of use; OA articles are governed by the applicable Creative Commons License

Overeem, I., & Syvitski, J. P. (2010). Shifting discharge peaks in Arctic rivers, 1977–2007. *Geografiska Annaler: Series A, Physical Geography*, *92*(2), 285–296. https://doi.org/10.1111/j.1468-0459.2010.00395.x

Palanques, A., Puig, P., Guillén, J., Jiménez, J., Gracia, V., Sánchez-Arcilla, A., & Madsen, O. (2002). Near-bottom suspended sediment fluxes on the microtidal low-energy Ebro continental shelf (NW Mediterranean). *Continental Shelf Research*, *22*(2), 285–303. https://doi.org/10.1016/S0278-4343(01)00058-9

Pickart, R. S., Spall, M. A., & Mathis, J. T. (2013). Dynamics of upwelling in the Alaskan Beaufort Sea and associated shelf-basin fluxes. *Deep-Sea Research Part I: Oceanographic Research Papers*, *76*, 35–51. https://doi.org/10.1016/j.dsr.2013.01.007

Pruszak, Z., Szmytkiewicz, P., Ostrowski, R., Skaja, M., & Szmytkiewicz, M. (2008). Shallow-water wave energy dissipation in a multi-bar coastal zone. *Oceanologia*, *50*(1), 43–58.

Rachold, V., Grigoriev, M. N., Are, F. E., Solomon, S., Reimnitz, E., Kassens, H., & Antonow, M. (2000). Coastal erosion vs riverine sediment discharge in the Arctic Shelf seas. *International Journal of Earth Sciences*, *89*(3), 450–460. https://doi.org/10.1007/s005310000113

Ranasinghe, R., Swinkels, C., Luijendijk, A., Roelvink, D., Bosboom, J., Stive, M., & Walstra, D. J. (2011). Morphodynamic upscaling with the MORFAC approach: Dependencies and sensitivities. *Coastal Engineering*, *58*(8), 806–811. https://doi.org/10.1016/j.coastaleng.2011.03.010

Reimnitz, E., Graves, S. M., & Barnes, P. W. (1985). Beaufort sea coastal erosion, shoreline evolution, and sediment flux (p. 78). *U.S. Geological Survey Open File Report, No: 85-380*.

Reimnitz, E., Graves, S. M., & Barnes, P. W. (1988). *Beaufort Sea coastal erosion, sediment flux, shoreline evolution, and the erosional shelf profile*. The Survey.

Reimnitz, E., & Maurer, D. K. (1978). Stamukhi shoals of the Arctic: Some observations from the Beaufort Sea. *US Geological Survey Open-File Report, No. 78-666*.

Reimnitz, E., Toimil, L., & Barnes, P. (1978). Arctic continental shelf morphology related to sea-ice zonation, Beaufort Sea, Alaska. *Marine Geology*, *28*(3–4), 179–210. https://doi.org/10.1016/0025-3227(78)90018-X

Roelvink, J. A., & Walstra, D. J. (2004). Keeping it simple by using complex models. *Advances in Hydro-Science and Engineering*, *6*, 1–11.

Ruggiero, P. (2013). Is the intensifying wave climate of the U.S. Pacific Northwest increasing flooding and erosion risk faster than sea-level rise? *Journal of Waterway, Port, Coastal, and Ocean Engineering*, *139*(2), 88–97. https://doi.org/10.1061/(asce)ww.1943-5460.0000172

Ruggiero, P., Buijsman, M., Kaminsky, G. M., & Gelfenbaum, G. (2010). Modeling the effects of wave climate and sediment supply variability on large-scale shoreline change. *Marine Geology*, *273*(1–4), 127–140. https://doi.org/10.1016/j.margeo.2010.02.008

Ruggiero, P., Kaminsky, G. M., Gelfenbaum, G., & Cohn, N. (2016). Morphodynamics of prograding beaches: A synthesis of seasonal-to century-scale observations of the Columbia River littoral cell. *Marine Geology*, *376*, 51–68. https://doi.org/10.1016/j.margeo.2016.03.012

Sepp, M., & Jaagus, J. (2011). Changes in the activity and tracks of Arctic cyclones. *Climatic Change*, *105*(3–4), 577–595. https://doi.org/10.1007/s10584-010-9893-7

Smith, M., & Thomson, J. (2016). Scaling observations of surface waves in the Beaufort Sea. *Elementa*, *2016*(1), 1–12. https://doi.org/10.12952/journal.elementa.000097

Sternberg, R. W., Berhane, I., & Ogston, A. S. (1999). Measurement of size and settling velocity of suspended aggregates on the northern California continental shelf. *Marine Geology*, *154*(1–4), 43–53. https://doi.org/10.1016/S0025-3227(98)00102-9

Stopa, J. E., Ardhuin, F., & Girard-Ardhuin, F. (2016). Wave climate in the Arctic 1992–2014: Seasonality and trends. *The Cryosphere*, *10*(4), 1605–1629. https://doi.org/10.5194/tc-10-1605-2016

Stroeve, J., Holland, M. M., Meier, W., Scambos, T., & Serreze, M. (2007). Arctic sea ice decline: Faster than forecast. *Geophysical Research Letters*, *34*(9), 1–5. https://doi.org/10.1029/2007GL0297-03

Sturtevant, P. M., Lestak, L. R., Manley, W. F., & Maslanik, J. A. (2004). Coastal erosion along the Chukchi coast due to an extreme storm event at Barrow, Alaska. In *Arctic Coastal Dynamics, Report of an International Workshop*.

Thieler, E. R., Brill, A. L., Cleary, W. J., Hobbs, C. H., & Gammisch, R. A. (1995). Geology of the Wrightsville Beach, North Carolina shoreface: Implications for the concept of shoreface profile of equilibrium. *Marine Geology*, *126*(1–4), 271–287. https://doi.org/10.1016/0025-3227(95)00082-A

Thomson, J., Fan, Y., Stammerjohn, S., Stopa, J., Rogers, W. E., Girard-Ardhuin, F., et al. (2016). Emerging trends in the sea state of the Beaufort and Chukchi seas. *Ocean Modelling*, *105*, 1–12. https://doi.org/10.1016/j.ocemod.2016.02.009

Thomson, J., & Rogers, W. E. (2014). Swell and sea in the emerging Arctic Ocean. *Geophysical Research Letters*, *41*(9), 3136–3140. https://doi.org/10.1002/2014GL059983

van der Wegen, M., Dastgheib, A., Jaffe, B. E., & Roelvink, D. (2011). Bed composition generation for morphodynamic modeling: Case study of San Pablo Bay in California, USA. *Ocean Dynamics*, *61*(2–3), 173–186. https://doi.org/10.1007/s10236-010-0314-2

van Rijn, L. C. (2007). Unified view of sediment transport by currents and waves. III: Graded beds. *Journal of Hydraulic Engineering*, *133*(7), 761–775. https://doi.org/10.1061/(asce)0733-9429(2007)133:7(761)

Wang, X. L., Feng, Y., Swail, V. R., & Cox, A. (2015). Historical changes in the Beaufort-Chukchi-Bering Seas surface winds and waves, 1971–2013. *Journal of Climate*, *28*(19), 7457–7469. https://doi.org/10.1175/jcli-d-15-0190.1

Warner, J. C., Sherwood, C. R., Signell, R. P., Harris, C. K., & Arango, H. G. (2008). Development of a three-dimensional, regional, coupled wave, current, and sediment-transport model. *Computers and Geosciences*, *34*(10), 1284–1306. https://doi.org/10.1016/j.cageo.2008.02.012

Weingartner, T. J., Danielson, S. L., Kasper, J. L., & Okkonen, S. R. (2009). Circulation and water property variations in the nearshore Alaskan Beaufort Sea (1999–2007).

Weingartner, T. J., Danielson, S. L., Potter, R. A., Trefry, J. H., Mahoney, A., Savoie, M., et al. (2017). Circulation and water properties in the landfast ice zone of the Alaskan Beaufort Sea. *Continental Shelf Research*, *148*, 185–198. https://doi.org/10.1016/j.csr.2017.09.001

Wiberg, P. L., Drake, D. E., & Cacchione, D. A. (1994). Sediment resuspension and bed armoring during high bottom stress events on the northern California inner continental shelf: Measurements and predictions. *Continental Shelf Research*, *14*(10–11), 1191–1219. https://doi.org/10.1016/0278-4343(94)90034-5

Wright, L. D. (2012). Recent advances in understanding continental shelf sediment transport. *Sediments, Morphology and Sedimentary Processes on Continental Shelves*, 159–172. https://doi.org/10.1002/9781118311172.ch8

21699291, 2022, 9, Downloaded from https://agupubs.onlinelibrary.wiley.com/doi/10.1029/2021JC018374 by Utrecht University Library, Wiley Online Library on [21/10/2022]. See the Terms and Conditions (https://onlinelibrary.wiley.com/terms-and-conditions) on Wiley Online Library for rules of use; OA articles are governed by the applicable Creative Commons License